Controls on river patterns in active tectonic settings in the central Italian Apennines

Master of Science thesis

Karen Tellefsen

Department of Earth Science
University of Bergen
2016

Acknowledgements

First of all I would like to thank my supervisor, the brilliant Patience Cowie, for giving me the opportunity to work with such an exciting project. You have consistently encouraged me to be confident in my own abilities, which made this project an experience in more than one way. Patience is a professor that does not only teach the curriculum to her students – she truly wants us all to really understand, which makes her very special. Working with you has been both educational and inspirational. Thank you so much!

Anneleen Geurts is thanked for being an invaluable help throughout the project. This includes help with ArcGIS and MATLAB, and excellent guidance during the field work in Italy. But also, for always having an open door, and answering my many questions, big or small. Thank you, Anneleen!

Ole Sannes Riiser was a great help in getting me started with the grain analyses in Adobe Photoshop. Håvard Fremgaard Fiksen also aided me initially with ArcGIS. Professor Jørgen Christian Meyer from the Institute of History at UoB helped with estimating the age of the dams along the stream, and Professor Kuvvet Atakan was a great help in my search for fault maps.

I would like to thank my mother, Inger Tellefsen, for help with proof reading, and friends and family for all their support.

I would also like to thank all my fellow geology students for five unforgettable years. A special thanks goes out to everyone at 'Hjørnerommet', for being the most wonderful support system. We have had so much fun and I will miss you all very much.

Last, but not least, I would like to thank Hallgeir Sirevaag. You were an excellent field assistant and private driver in Italy. Your guidance with LyX and Adobe Illustrator has been most helpful, as well as your meticulous proof reading. But most of all, you have been extraordinarily patient and kind to me for the past two years, and I am looking forward to returning the favour when you are finishing your Ph.D. And as a geologist, I now feel absolutely confident in stating the following: you are my rock.

Bergen, 31 May 2016

Karen Tellefsen

Abstract

The central Italian Apennines have gone through a complex evolutionary history, involving compression and subsidence, followed by extension and uplift. The last 3 Ma, the area has experienced active extension, and presently features a wide belt of parallel active normal faults. The configuration and evolution of the drainage network is largely controlled by activity along these faults, along with regional uplift. The central Apennines therefore represent an excellent site for studying the relations between fluvial geomorphology and tectonics.

This study presents detailed data from two catchments in central Italy, containing highly active normal faults, one of which intersects the Paganica Fault that caused the devastating M_w 6.3 earthquake in 2009. This study aims to determine whether or not the studied streams are transiently responding to increasing slip rates on the faults they intersect, and if the two catchments might be interacting, with the overall goal of increasing our understanding of the landscape dynamics within the Abruzzo Region. Whether or not the study of fluvial geomorphology could aid in the prediction of high magnitude earthquake events, is also discussed.

Data has been acquired through digital analyses by use of a high-resolution digital elevation model, and through detailed field work in the Abruzzo Region. Most of thse obtained data indicate a transient response for both streams, with some exceptions. The length–area-correlation turns out to be particularly interesting, as it provides linear plots with a Hack's constant that strongly indicates topographic steady state for both streams. This is discussed to be an indication that Hack's law is inadequate for determining whether or not a natural fluvial system is in equilibrium. Another possibility is that Hack's law is a delayed feature within the drainage systems, reflecting paleotopography, and the state of the catchments prior to faulting.

Capturing events caused by aggressive headward erosion by streams intersecting active normal faults seems to be among the main processes in which the stream network is evolving within the field area. It is possibly the shaping mechanism for the studied catchments, and will likely be just as important for the future evolution of the drainage network within the central Italian Apennines.

Contents

1 Introduction

The central Italian Apennines have experienced a complex tectonic history, involving compression, followed by extension and regional uplift. Over the last 3 Ma, the area has been subject to active extension, and currently features a wide belt of parallel active normal faults. The configuration and evolution of the drainage network in the region is influenced by activity along these faults, along with the regional uplift. The central Apennines therefore represent an excellent site for studying the relations between fluvial geomorphology and tectonics. This study presents detailed data from two catchments in central Italy, containing active normal faults. The data has been acquired through digital analyses by use of a high resolution digital elevation model, and through detailed field work in the Abruzzo Region.

1.1 Research objectives

Can tectonic signals be inferred from studying fluvial geomorphology? Rivers respond to changes in external boundary conditions, which may be caused by tectonic activity. As fluvial erosion rate is affected by fault movements, the river channels evolve, thus being able to transfer these signals to the nearby hillslopes, and ultimately, the surrounding landscape. Consequently, it is theoretically possible to trace fault activity by investigating rivers. Fluvial geomorphologists have developed several fluvial scaling relationships – models – describing relations between different river attributes. However, studies have shown that these relationships may break down for rivers undergoing changes in external boundary conditions (e.g. an increase in tectonic activity). To determine if a stream might be affected by an active normal fault, one must therefore investigate these fluvial scaling relationships, which is among the main purposes of this study.

The central Italian Apennines contain a network of mainly parallel, high-angle active normal faults, making it a highly tectonically active area. Major earthquakes have impacted the area, the most recent one was a M_w 6.3 earthquake in L'Aquila in 2009. The surface rupture was found on the little known Paganica Fault, which had only recently been mapped as an active structure. This fault lies within the Paganica Catchment, thus the stream that intersects the Paganica Fault is ideal for studying the relationship between stream morphology and active tectonics. Whittaker et al. (2007a; 2007b) showed how rivers may display traces of active tectonics, two years before the devastating event in 2009. This poses the following question: by following the approaches of Whittaker et al. (2007a; 2007b) for the stream intersecting the Paganica Fault, would it have been possible to forsee the potential for such a damaging earthquake?

Less than 1 km from the headwaters of the Paganica Catchment lies the Barete Catchment, containing the active Montereale and Barete faults, that are also intersected by a stream. Could these catchments be interacting? The two catchments are highly similar in terms of area, stream length and the appearence of active normal faults. This study aims to investigate the similarities

and differences of these two catchments, and determine whether they are in topographic steady state, in an attempt to better understand the dynamics within this tectonically active area.

1.2 Study area

The Pescara Catchment (Fig. 1) is among the major catchments in the central Italian Apennines (>3000 km^2). The catchment is located within the provinces of L'Aquila and Pescara of the Abruzzo Region, forming a triangular shape as the Aterno River runs from Montereale in the northwestern corner, towards the southeast and then northeast through the Popoli Gorge (after which it is called the Pescara River) and drains into the Adriatic Sea in the city of Pescara. The study area includes two of the many sub-catchments within the Pescara Catchment, both located in the northwestern corner, known as the Paganica and Barete catchments.

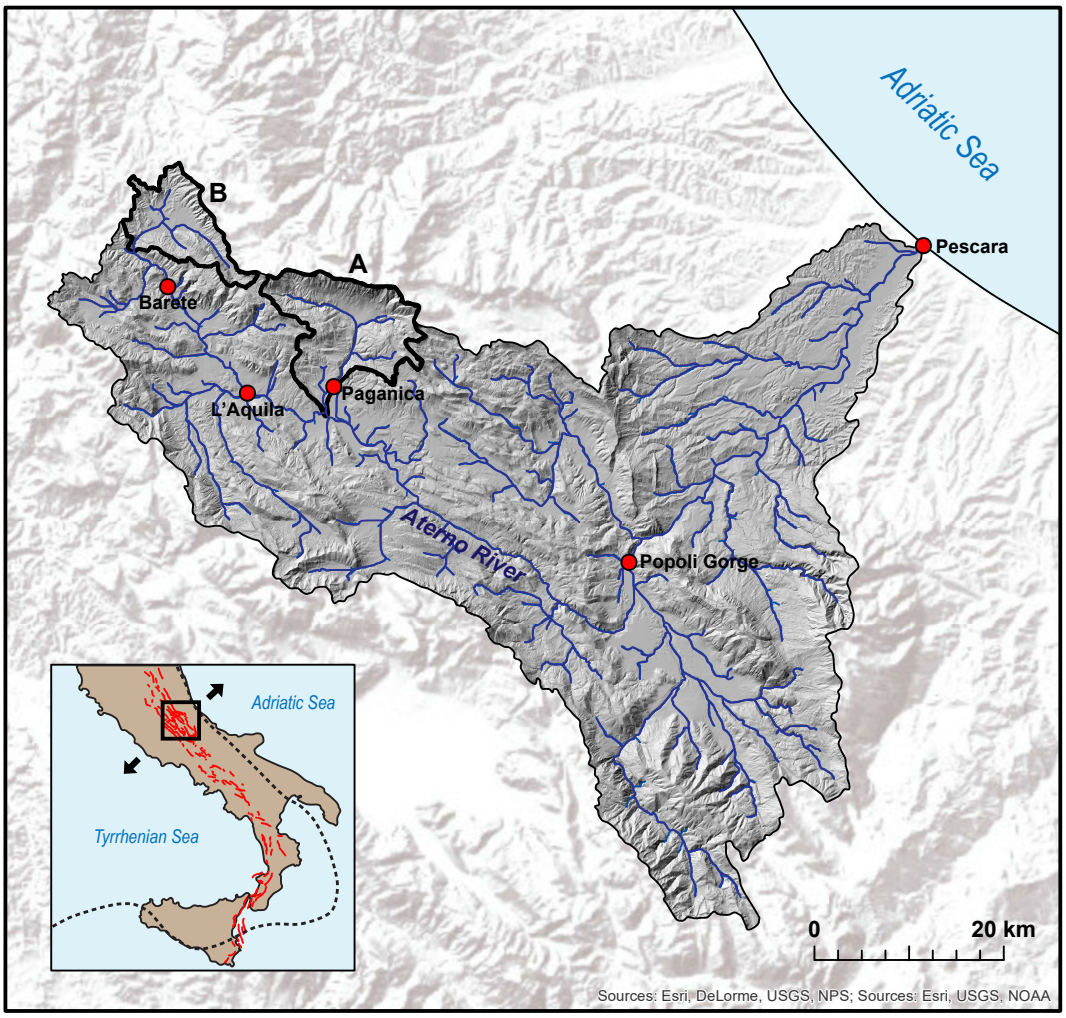

Fig. 1: Hillshade map showing the Pescara Catchment with its drainage network. The studied catchments are outlined in the northwestern corner (A = Paganica, B = Barete). The smaller map of Italy contains the normal fault array (red lines), the thrust front (dashed line) and the location of the Pescara Catchment is indicated with a black square.

1.2.1 The Paganica Catchment

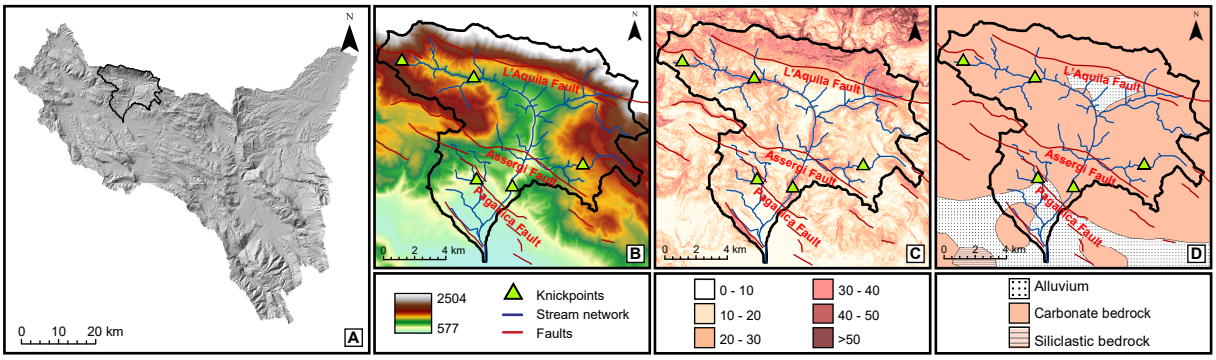

Fig. 2: **A:** Hillshade map based on the Pescara DEM (Tarquini et al., 2012), showing the location of the Paganica Catchment within the Pescara Catchment. **B:** 10-m DEM displaying the topography of the Paganica Catchment. **C:** Slope map calculated based on the DEM, highlighting the location of steep hillslopes within the catchment. **D:** Lithological map featuring the exposed bedrock within the catchment (source: isprambiente.gov.it). Possible knickpoints are indicated by green triangles and the stream network is indicated by blue lines. The fault array indicated by red lines is by Roberts and Michetti (2004).

The Paganica Catchment (Fig. 2) is located near the northwestern corner in the Pescara Catchment, approximately 5 km northeast of the city of L'Aquila. The Paganica Catchment has a drainage area of almost 140 km^2, and the studied stream segment is 20 km long. The drainage pattern within the catchment is dendritic. The studied stream segment starts in the northwestern corner and turns south through the villages of Assergi and Camarda (after which it is known as the Raiale River), through the town of Paganica, before joining the Aterno River. For simplicity, the studied river segment will be referred to as the 'Paganica Stream' from this point on.

The Paganica Catchment has a varied topography from highly elevated, mountainous areas, valleys and smaller gorges, to flat farmland areas. The northern edge of the catchment is the southern boundary of the Gran Sasso Mountains, the highest mountain chain within the Apennines. Here, catchment elevations are well over 2000 masl, whereas the confluence point after the town of Paganica is below 580 masl. The lithology mainly consists of carbonate bedrock, but with patches of alluvium in the central and confluence areas.

Normal faults are found within both studied catchments, most with a main strike of northwest–southeast, on which several major normal faulting earthquakes have occurred during modern times (e.g. Cinti et al., 2011). The largest normal fault within the Paganica Catchment is the L'Aquila Fault, located along the northern boundary of the catchment, which has slip rates exceeding 1 mm/yr at the fault centre (Roberts and Michetti, 2004). The Paganica Stream normally intersects two other faults: the Assergi Fault, a seldom mapped feature for which there is little data available, and the Paganica Fault (part of the Paganica San-Demetrio fault system) (Blumetti et al., 2013).

The most recent normal faulting event in the central Apennines was caused by the Paganica Fault, in the city of L'Aquila, April 6th, 2009. The fault ruptured, resulting in an earthquake of M_w 6.3 that caused over 300 casualties and extensive damage to L'Aquila and several surrounding villages. As previously stated, the area is well documented in terms of faults and tectonic activity. However, before 2009, the Paganica Fault was a little known structure, and to find the surface rupture on such a feature rather than some of the larger faults in the area was a challenge to many (e.g. Galli et al., 2010). The fault was identified as a late-Quaternary fault by Bagnaia et al. (1992, in Blumetti et al., 2013), and later mapped as a 13 km long, active feature by Pace et al. (2006), only three years before the devastating event. Their seismic hazard analyses then estimated that the Paganica Fault would be capable of producing earthquakes with a maximum magnitude of 6.3. The Paganica Fault was assigned a slip rate of 0.6 mm/yr, and three other earthquake incidents with $M_w \geq 5$ in 1461, 1762 and 1958 were listed (Pace et al., 2006). Later research has estimated slip rates mainly between 0.4–0.5 mm/yr (Galli et al., 2010; Cinti et al., 2011; Blumetti et al., 2013), and throw rates between 0.3–0.4 (Roberts et al., 2010).

1.2.2 The Barete Catchment

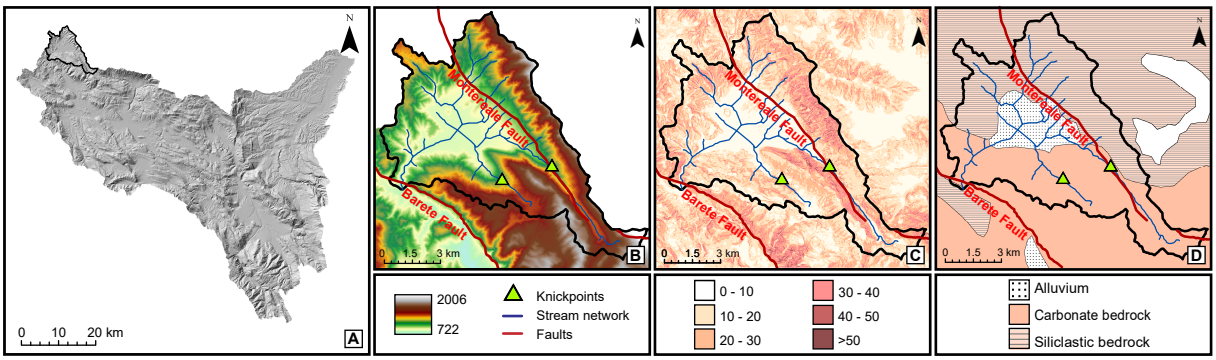

Fig. 3: **A:** Hillshade map based on the Pescara DEM (Tarquini et al., 2012), showing the location of the Barete Catchment within the Pescara Catchment. **B:** 10-m DEM displaying the topography of the Barete Catchment. **C:** Slope map calculated based on the DEM, highlighting the location of steep hillslopes within the catchment. **D:** Lithological map featuring the exposed bedrock within the catchment (source: isprambiente.gov.it). Possible knickpoints are indicated by green triangles and the stream network is indicated by blue lines. The fault array indicated by red lines is by Roberts and Michetti (2004)

The Barete Catchment (Fig. 3) is located north of the town of Barete, which lies about 15 km northwest of the city of L'Aquila. The catchment makes up the northwestern corner of the Pescara Catchment, the total drainage area is nearly 80 km^2 and the drainage pattern is dendritic. The studied stream segment is about 18 km long and runs from the northeastern corner of the catchment, before turning south through the villages Capitignano and Piedicolle towards the village Marana (ca. 6 km northwest of Barete), in which the stream becomes known as the Aterno River. The upstream river segments are mapped with several names:

F^so Faschiano, *T. Mozzana* and *Rio Riano* (Appendix 6, Vezzani and Ghisetti, 1998), but for simplicity the studied segment will be referred to as the 'Barete Stream' from this point on.

The Barete catchment has a topographic relief of about 1200 m, with highest elevations in the headwaters close to 2000 masl, and lowest elevations near the village Marana of 780 masl. The topography varies from very flat farmland areas to steeper, mountainous areas. The Gran Sasso Mountains are found only a few kilometres northeast of the headwater area. The catchment contains three main lithologies: carbonate bedrock, alluvium and siliciclastic bedrock (flysch).

The Barete Catchment contains the Montereale Fault, a 16.2 km long structure (Pace et al., 2006) which the headwaters of the Barete Stream may be intersecting at its southeastern tip. The fault caused a M_w 6 earthquake in January 1703, and M_w 6.4 is believed to be the largest earthquake this fault can produce (Pace et al., 2006). A more well-known structure is the Barete Fault (also called the Mt. Marine Fault); a 20.5 km long active normal fault estimated to have initiated at 2.91 Ma (Roberts and Michetti, 2004). The most recent rupture on this fault was in February, 1703, causing an earthquake of M_w 6.7 (Galli et al., 2011). On maps by Roberts and Michetti (2004) and Papanikolaou et al. (2005), the stream intersects the Barete Fault at its nothwestern tip. Here, the throw rate is believed not to exceed 0.3 mm/yr, whereas the fault center (9 km southeast) has an estimated throw rate of 0.55±0.2 mm/yr (Roberts and Michetti, 2004; Papanikolaou et al., 2005). Galli et al. (2011), however, does not draw this fault far enough to the northwest for it to be interacting with the Barete Stream, i.e. the river crosses very near the fault tip.

The Barete Fault and the Paganica Fault have been recognized as parts of a large, segmented fault system (the L'Aquila faults), which can rupture entirely or partially to generate earthquakes of different magnitudes (Galli et al., 2011).

2 Background

This chapter features the geological history of the central Apennines, along with more detailed descriptions of its lithology, tectonics and fluvial system. A theoretical section is included, introducing the term of transience and explaining different fluvial scaling relationships used in methods of geomorphological modelling.

2.1 Geological history

The western Mediterranean area has experienced a protracted complex tectonic history owing to the opening and closing of the Tethyan ocean, involving the Eurasian and African plates, along with numerous microcontinents (e.g. Malinverno and Ryan, 1986; Stampfli, 2000; D'Agostino et al., 2001; Roberts and Michetti, 2004). From late Oligocene to Pliocene times, the central Italian Apennines were affected by compression and thrusting during the final stages of the closing of the Neotethys Sea (Gueguen et al., 1998). The Adriatic microplate was subject to westward subduction beneath the eastern margin of Italy, causing SW-directed reverse faulting over most of the peninsula, as well as flexural subsidence caused by orogenic loading (Patacca et al., 1990; Gueguen et al., 1998). The subduction is referred to as passive subduction, where the old and dense Adriatic lithosphere pulled on the rest of the subducting plate, causing eastward roll-back of the Calabrian subduction zone (Fig. 4) (Malinverno and Ryan, 1986; Patacca et al., 1990).

During Pliocene times, the compressional forces migrated eastwards with the subduction zone, and extension followed immediately after behind the compressional front. Plate convergence slowed down, flexural subsidence was replaced by regional uplift, and normal faults began to form (e.g. Lavecchia et al., 1994; D'Agostino et al., 2001; Centamore and Nisio, 2003). This uplift has been interpreted as a result of slab break-off and mantle convection, hence the central Apennines are within a slab window where active subduction has ceased (Faccenna et al., 2014). This sequence of events has resulted in an imbricate fold and thrust belt (e.g. D'Agostino et al., 2001; Roberts and Michetti, 2004) lying atop a long-wavelength (150–200 km) topographic bulge oriented N–S along the peninsula (D'Agostino et al., 2001). The northern and southern Apennines are presently dominated by compression and subsidence, while the central part is dominated by extension and uplift (Faccenna et al., 2014). The simultaneous occurrence of extension and regional uplift within the central part of the topographic bulge has led to the creation of numerous, fault-bounded half-graben basins, many of which have been internally-draining in the past (D'Agostino et al., 2001). In these basins, local subsidence is caused by active normal faulting, while headward erosion is induced by regional uplift and base level fall at the coast (D'Agostino et al., 2001).

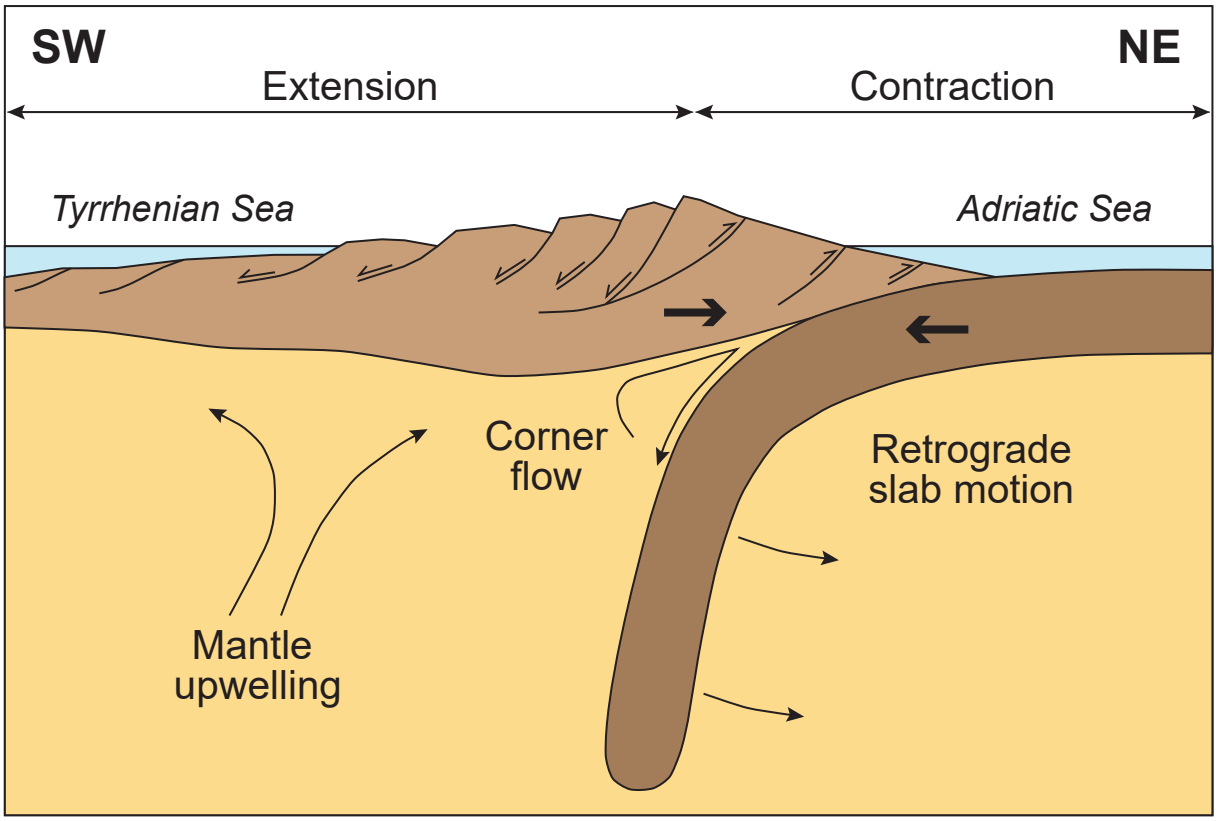

Fig. 4: The central Italian Apennines are affected by extension and uplift (mantle upwelling) as the rollback of the subducting Adriatic slab (retrograde slab motion) has led the compressional front to migrate east. Modified after Cavinato and De Celles (1999).

2.2 Lithology of the central Apennines

The bedrock sequence of the Apennines is dominated by stacked thrust units with resistant limestones of Jurassic to Paleocene age and less resistant, formerly deformed turbidite flysch of Upper Miocene age (Cavinato et al., 1994; Centamore and Nisio, 2003). These units have been previously deformed by Neogene thrusting (Bigi et al., 1992 in D'Agostino et al., 2001). The half-graben basins contain continental deposits from Late Pliocene and onwards, that are considered nearly contemporaneous with the onset of extension across the Apennines (Cavinato, 1993; Centamore and Nisio, 2003). These are coarse-grained breccias and conglomerates, alluvial sequences, and lacustrine, deltaic and fluvial deposits, sometimes with interbedded volcanics (Cavinato, 1993). The sequences reflect a history of dynamic uplift and varying erosion rates, controlled by active tectonics and changing climatic conditions (Centamore and Nisio, 2003).

2.3 Tectonic setting and seismicity

The central Apennines are presently undergoing NW–SE extension along with regional uplift (e.g. Patacca et al., 1990; Cavinato and De Celles, 1999; D'Agostino et al., 2001), resulting in a ca. 150 km long network of relatively high-angle (>45°) active normal faults, some of which

overprint previous thrust structures (Centamore and Nisio, 2003; Roberts and Michetti, 2004). This extensional fault array is well constrained in terms of variation in displacement and slip rate, both between faults and along individual segments (Whittaker et al., 2007b).

The faults are soft-linked, demonstrate nearly pure dip-slip movement (Roberts and Michetti, 2004) and accommodate extension of about 3.9 ± 0.8 mm/year across central Italy (Papanikolaou et al., 2005). Offsets decrease towards the fault tips (Cowie and Roberts, 2001; Roberts and Michetti, 2004), and the throw and throw rates are highest for the central faults within the normal fault array (Cowie and Roberts, 2001). Temporal variations in the fault slip rates have been demonstrated by Cowie and Roberts (2001), where acceleration in fault throw rates have been interpreted as a result of fault growth and interaction. An acceleration in the throw rates occurred at ~ 0.75 Ma for the central faults, whereas the distal faults have moved at constant rates over the last 3 Myr (Cowie and Roberts, 2001; Roberts and Michetti, 2004). As mentioned in the previous chapter, the two studied catchments have experienced several major normal faulting earthquakes during modern times.

Seismicity in the central Apennines is concentrated along the area of highest elevations (Anderson and Jackson, 1987; Amato et al., 1997 in D'Agostino et al., 2001) on normal faults that overprint previous compressional structures (D'Agostino et al., 2001). In the northern and southern Italy; the active seismic belt is only 20–30 km wide (Valensise and Pantosti, 2001 in D'Agostino et al., 2001), whilst in the central Italian Apennines (between 41.5 and 42.5 degrees N), the belt is estimated to be at least 50 km (D'Agostino et al., 2001) and possibly even 90 km wide (Cowie et al., 2013).

2.4 Evolution of the drainage networks

The drainage networks of central Italy can be divided into two major systems: an integrated stream network along the flanks of the Apennines, and the previously internally-draining half-graben basins along the main watershed (D'Agostino et al., 2001). The Aterno-Pescara river system, in which the studied rivers are found, is an example of the first drainage system type. The catchment is located upstream of the Popoli Gorge and drains an area of over 3000 km^2.

Within a catchment, the configuration of the drainage network, and thereby erosion rate and sedimentation, is largely controlled by fault movement and regional uplift (D'Agostino et al., 2001). Cowie et al. (2006) modelled some of these mechanisms, showing how fault array growth influences surface processes and ultimately contributes to catchment development. The stratigraphy of the basins show an evolution from low-gradient fluvial and lacustrine deposits to steeper-gradient braided alluvial-fluvial fan deposits that often incise earlier sediments. This indicates that the Quaternary drainage evolved from an internally-drained system to a through-going river network which frequently cut through and captured other internally-draining basins (D'Agostino et al., 2001). As a consequence, the Fucino and Colfiorito basins are likely to be the only internally drained basins at present (D'Agostino et al., 2001). For the Aterno-Pescara system, this development took place when drainage through the Popoli Gorge started. This

caused river incision to increase and triggered regressive or headward erosion in the upstream basins, reorganizing the drainage network by capturing other basins. These changes have been interpreted as a result of fall in regional base level, ultimately related to regional uplift induced by mantle upwelling beneath the Apennines (D'Agostino et al., 2001). Evidences for stream capturing are observed throughout the Pescara Catchment as large windgaps.

In short, the most important factors in the evolution of the drainage network and sedimentation in the intermontane basins has been the interaction of regional uplift caused by mantle upwelling, and local subsidence caused by active normal faulting (D'Agostino et al., 2001).

2.5 Landscape transience

A landscape in equilibrium or topographic steady state has a fixed base level, climate and lithology, and tectonic activity is at a steady rate (Whipple, 2001, and references therein). Consequently, the rates of uplift and erosion are in perfect balance, and the erosion rate is constant throughout the stream (e.g. Whipple, 2004). This produces a graded, concave river profile (Fig. 5A), where the channel slope decreases, channel width widens and the drainage area increases steadily downstream. Rivers in topographic steady state are best described by a transport-limited model, where erosion rate depends on the capacity of the river to transport sediment (Attal et al., 2011). The plotting of fluvial scaling relationships for equilibrium rivers has also been found to follow certain trends, which will be reviewed in section 2.6.

If, however, the rates of uplift vary throughout the catchment, there will be a mismatch in response time between the river and its surrounding hillslopes, leading to a transient or non-steady state behaviour (Whipple, 2001; Castillo et al., 2013). This produces short-term and unstable landforms and often the formation of knickpoints – kinks in the river profile (Fig. 5B). Knickpoints may develop because of a sudden fall in base level, which can be induced by eustatic or isostatic changes, tectonic activity, changes in water or sediment flux, river capture, or a change in lithology (Whipple, 2004; Castillo et al., 2013). Hence, knickpoints may indicate a landscape in transience, i.e., a landscape still adjusting to external forcings. Transiently responding rivers are best described by a detachment-limited model, where erosion rate depends on the ability of the river to remove rock fragments from the channel (Attal et al., 2011). Whether or not a landscape is a transient state can be determined by studying bedrock incision rates, changes in sediment size and variations in channel width (Castillo et al., 2013, and references therein).

As previously mentioned, the central Italian Apennines have, during the last ca. 3 Ma, undergone a change from compression and subsidence to extension and uplift, along with a range of different climatic conditions. This has led to varying fault slip rates through time, and a dynamic development of the drainage network. Adjusting to external boundary conditions and reaching topographic steady state may take millions of years (Whittaker et al., 2008). Therefore it is reasonable to assume that the central Italian Apennines are presently in a transient state.

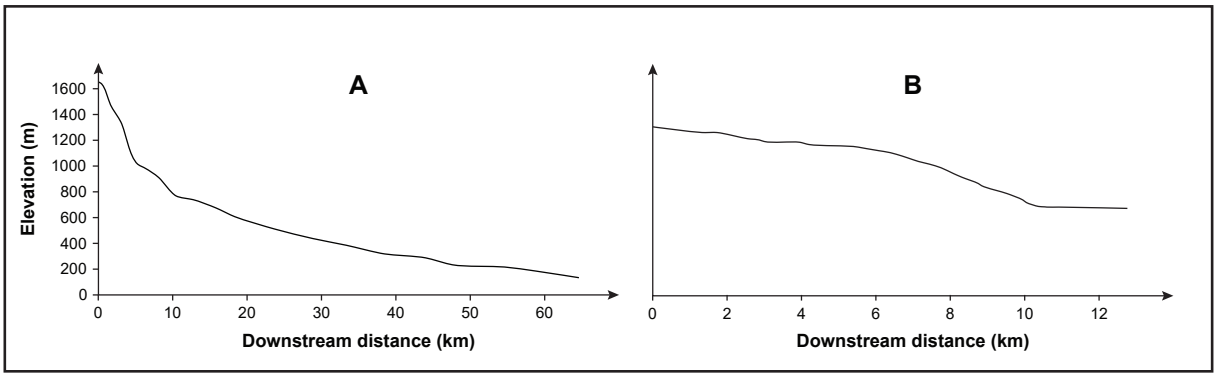

Fig. 5: **A:** Longprofile of the Penaro River in northern Italy, an example of a river in equilibrium. The graded, concave-up profile is typical for streams in a steady state condition. **B:** Longprofile for the Rio Torto River in central Italy, a transiently responding river. The profile displays a clear convex reach, a knickpoint, which is a typical feature for rivers in a non-steady state. The profiles are based on lecture material from the course Geodynamics and Basin Modelling (GEOV254) at the University of Bergen.

2.6 Fluvial scaling relationships

Models describing relationships between rivers and external forcings (e. g. erosion, uplift) will in this study be used for comparison with the data obtained through field work and computer analyses. Prior to this step, a range of different factors must be calculated.

Measurements of bankfull channel width, W_b, and depth, H_b, may be used to calculate the hydraulic radius, R_h, of a stream:

$$R_h = \frac{Cross - sectional\,area\,(m^2)}{Wetted\,perimeter\,(m)} \tag{1}$$

where $cross - sectional\,area = W_b H_b$ and $wetted\,perimeter = W_b + 2H_b$. R_h may further be used together with slope measurements (S) to calculate bed shear stress, τ_b, describing the force exerted by clear, flowing water on the channel bed in N/m^2:

$$\tau_b = \rho_w g R_h S \tag{2}$$

where ρ_w is the density of water and g is the gravity constant. When a critical bed shear stress is reached, the stream is able to put sediment in motion. This is defined by the dimensionless Shields stress, τ^*:

$$\tau* = \frac{\rho_w R_h S}{(\rho_s - \rho_w)\, D_{50}} \tag{3}$$

where ρ_s is the density of sediment and D_{50} is the median grain size obtained by digital analysis of sediment photos taken at active gravel bars along the stream. This parameter depends largely on the size of the sediment and thus describes the control sediment size has on channel slope (Whittaker et al., 2007b). For gravel-bed or transport-limited rivers where there is a strong relationship between grain size and slope, the τ^*_{cr} values commonly lie between 0.047–0.06 (Whittaker et al., 2007b, and references therein).

Shear stress scales with unit stream power (or specific stream power), determining the stream capacity per unit channel width (W/m^2):

$$USP = \frac{AS}{W_b} \tag{4}$$

where A is area in m^2, S is slope in m/m, and W_b is channel width in m.

Hack's law provides the empirical relationship between stream length (L) and the related drainage area (A). In a log-log plot, these parameters should make a linear plot from which Hack's constant, h (the power law exponent), can be found. For a river in dynamic equilibrium drainage area increases with downstream distance and h should be close to 0.6 (Hack, 1957)(Fig. 6A).

$$L \propto A^h \tag{5}$$

Channel width (W) also scales with drainage area and normally increases with downstream distance. A log-log plot of drainage area against channel width provides the channel width scaling exponent, α, which, for an equilibrium river should be close to 0.5 (Fig. 6B).

$$W \propto A^\alpha \tag{6}$$

Along with stream length, Hack's constant, and two other constants C (integration constant) and K (erodibility), α may be used to calculate new elevations, and thereby model stream long profiles for equilibrium rivers:

$$H = -\frac{K \times l^{(1-p)}}{(1-p)} + C \tag{7}$$

where H is the new elevation in m, and $p = \frac{1-\alpha}{h}$.

Channel slope (S) scales negatively with drainage area, as slope tends to decrease downstream for a river in equilibrium. A log-log plot of drainage area against slope provides the concavity index, θ, which ranges from $\sim$ 0.2 to 1.0, and is usually close to -0,5 for a river in equilibrium (Zaprowski et al., 2005, and references therein; Tarboton et al., 1991 and Sklar and Dietrich, 1998 in Kirby and Whipple, 2001) (Fig. 6C).

$$S \propto A^{-\theta} \tag{8}$$

Aspect ratio (W_b/H_b) may also be plotted against slope to provide information on how a stream modifies its dimensions in response to changing channel steepness.

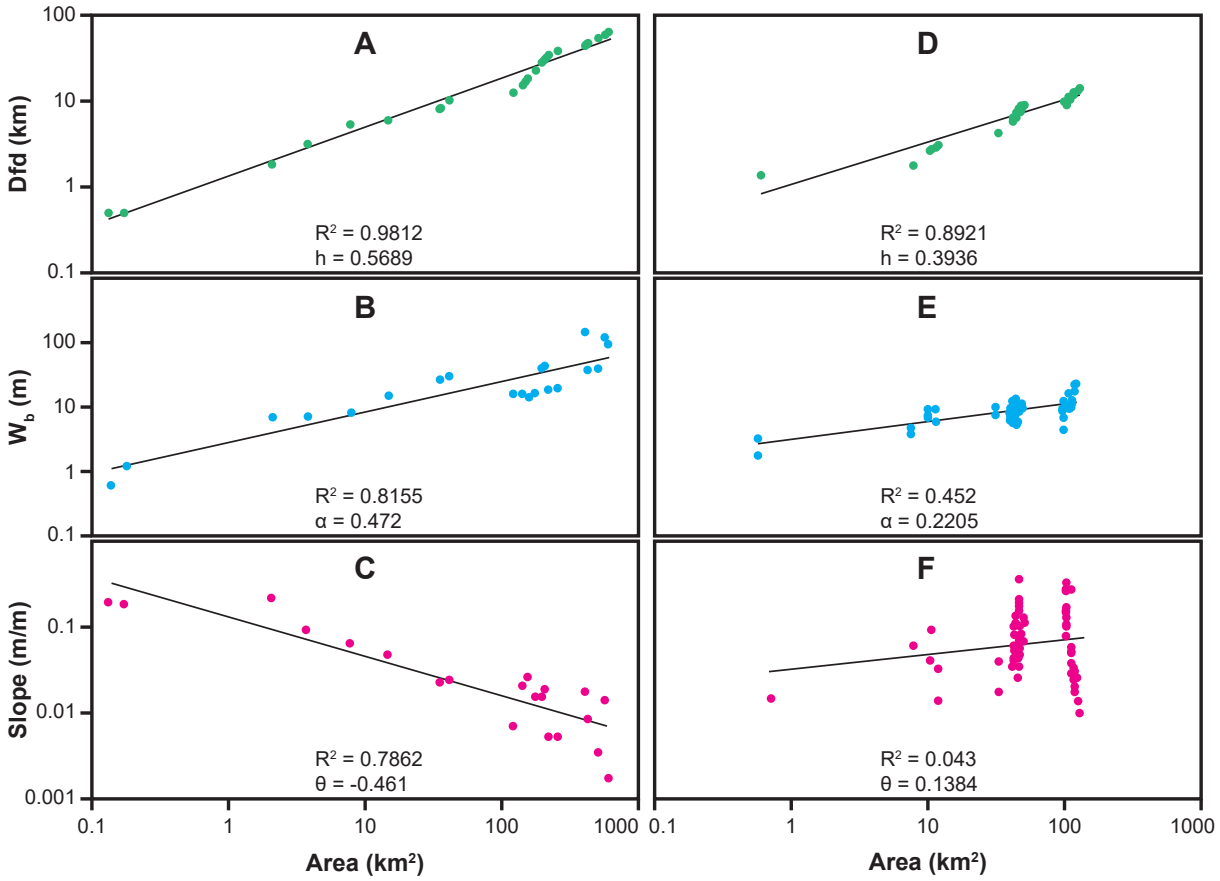

Fig. 6: Plotting of different fluvial scaling relationships for the Penaro River in topographic steady state (A, B, C), and for the transiently responding Rio Torto River (D, E, F). **A:** The length–area-correlation for a river in equilibrium should provide a Hack's constant (h) close to 0.6. **B:** The width–area-correlation for a river in equilibrium should provide a power-law exponent (α) close to 0.5. **C:** The slope–area-correlation for a river in equilibrium should provide a concavity index (θ) close to -0.5. For the transiently responding Rio Torto River, the plots are very different: the exponents h (**D**), α (**E**) and θ (**F**) are far from the idealised values for a stream in equilibrium. For the Rio Torto, the concavity plot is observed to be particularly scattered.

The equations and relations above provide insight in fluvial scaling relationships that mostly apply to rivers in dynamic equilibrium. However, for rivers undergoing a transient response to external forcing, many of these scaling relationships break down and no longer accurately describe the state of the river (Whittaker et al., 2007a). This study aims to further examine these aspects in order to determine the dynamic state (transient or equilibrium) within the Paganica and Barete catchments.

3 Methods

The research for this study is divided into three main parts: data preparation prior to field work, field observations and data processing. These stages will be explained in the following sections. The approaches are largely based on the applied methods in Whittaker et al. (2007a,b, 2008, 2010) and Cowie et al. (2008), as these studies deal with similar issues.

3.1 Data preparations

Initial DEM (digital elevation model) analyses of the Pescara Catchment were done at the University of Bergen, providing the basis for further analyses. The Pescara DEM (Tarquini et al., 2012) displays an area of 3153 km^2 and has a resolution of 10 m. The DEM analyses were used to build stream networks (Fig. 7) and extract watersheds (Fig. 8), using *ArcGIS* 10.2-3.

First, the DEM was prepared for further analyses by filling in sinks or potholes to create a hydrologically consistent surface (Fig. 7A). This "smoothed" DEM was used to extract a flow direction raster (Fig. 7B), from which calculations of flow accumulation were made (Fig. 7C). Then, the stream network was defined. The flow accumulation raster was used as input and an accumulation value of >10.000 was set as the drainage threshold for stream formation. Only pixels having more than 10 000 pixels draining into them were visualised as streams. After stream ordering, the final stream network raster was converted into a vector feature (Fig. 7D).

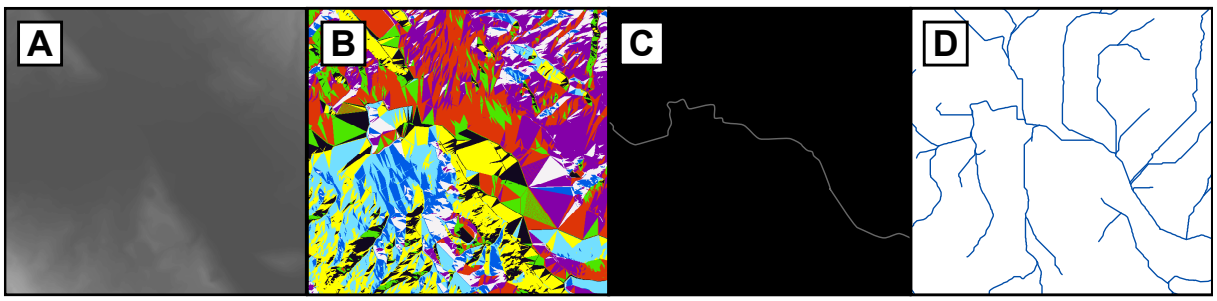

Fig. 7: Overview of the different steps in the process of creating a drainage network from the DEM (Tarquini et al., 2012). **A:** Initial DEM after filling sinks and potholes. **B:** Flow direction raster, **C:** Calculated flow accumulation raster. **D:** Final stream network.

Next, sub-catchments within the north-western and southern parts of the Pescara Catchment were extracted. Pour points were defined and placed on the tributary streams just upstream of the confluence point with the main river (Aterno River). Then, by using the flow direction raster and pour points as input, the "Watershed" tool was used to define all pixels draining into one pour point as a separate watershed. Thus, sub-catchments within the Pescara Catchment were visualised (Fig. 8).

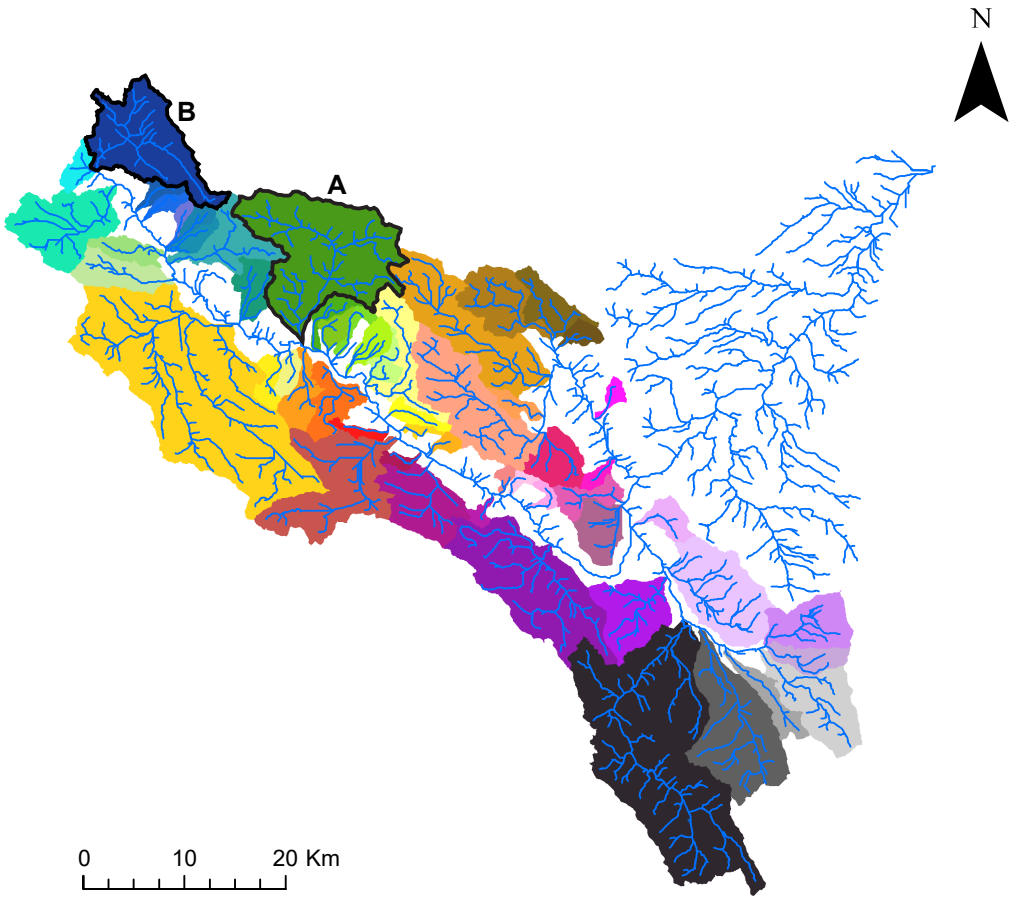

Fig. 8: Using a digital elevation model as input (Tarquini et al., 2012), ArcGIS was used to calculate the stream networks (blue lines) and subcatchments (coloured areas) within the Pescara Catchment. The studied sub-catchments (Paganica = A and Barete = B) are outlined in the upper left corner.

MATLAB (R2015b) was used to extract stream longprofiles from the DEM (Fig. 9). Stream longprofiles from the different sub-catchments were studied in detail and compared to two lithological maps of different resolutions: a detailed map by Vezzani and Ghisetti (1998) (Appendix 6), and a less detailed map by Tarquini et al. (2012), along with the fault map by Roberts and Michetti (2004) (Fig. 2D and 3D). Based on observations of the stream profiles in relation to the lithological maps, two sub-catchments were selected to be studied further: the Barete and Paganica catchments (Fig. 8). Both are among the larger sub-catchments of the area, both streams contain longprofile convexities and both intersect active normal faults, one of which caused the M_w 6.3 earthquake in L'Aquila in 2009. Hence, these catchments – being in a highly tectonically active area – were considered to be of particular interest. The catchments are similar in shape and size, and the two streams appear almost symmetrical in map view. Additionally, their close proximity (<1 km between the headwaters) means similar elevations and climatic conditions. As the time limitation of the field work did not allow for high-resolution studies of both catchments, the Paganica Catchment was chosen to be studied in more detail.

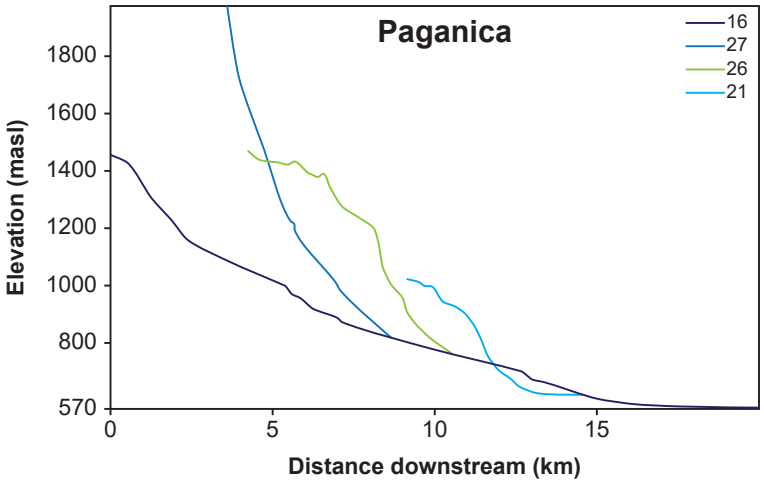

Fig. 9: Example of stream profiles extracted in MATLAB by using the DEM (Tarquini et al., 2012) as input. Here; the Paganica Catchment. The longest segment of the river (16; the studied segment) starts near the water divide in the north-western corner of the catchment. Three large tributaries then follow (27, 26 and 21). Segment 16 appears to contain three minor convexities.

3.2 Field methods

Field work started in Paganica, where data was collected along $\sim 80\,\%$ of the stream length. The high-resolution data collection started near the water divide in the north-western corner of the catchment, and continued downstream. GPS position and -elevation were taken at each locality, as well as observations on bankfull channel width and depth, along with descriptions of the near-channel area regarding topography, vegetation, sediments and/or exposed bedrock. At localities with gravel bars, detailed photos of representative sediments were taken for later grain analyses. In the Barete Catchment, data collection started further downstream and continued towards the headwaters. Data collection was more sporadic and less detailed than in Paganica, and the channel was difficult to reach in the upstream areas. Therefore there is a gap in data collection in the headwaters of the Barete Stream. More detailed descriptions of the field work follow below.

3.2.1 Defining bankfull stage

Bankfull stage is the flooding stage of a river. It is the maximum discharge that can be contained within the channel, before water starts spilling onto the flood plain. The width and depth of the channel at bankfull discharge is termed the bankfull width and bankfull depth (Charlton, 2007). Determining these parameters in nature can be challenging. Bankfull stage may be indicated by a break in topography where the sloping active channel meets the horizontal floodplain. Lines of trees or a sharp break from no vegetation to dense vegetation can also be an indicator. Lastly, a sudden change in sedimentology from coarse-grained to fine-grained, or bleaching on boulders, may indicate bankfull stage (Whittaker et al., 2007a).

3.2.2 Laser measurements

Detailed profiles were made along the stream at every kilometre on average, with higher frequency where the surroundings allowed for it. As the streams were quite narrow, the 10-m-resolution DEM would obscure the more detailed topography. A laser rangefinder (TruPulse 360) was therefore used to make high resolution profiling, aid in determining bankfull channel width and -depth, and to measure local slope (Fig. 10). The instrument uses a laser beam to determine the horizontal and vertical distance to an object, along with direct distance, inclination and azimuth.

Fig. 10: Profiling by the use of a laser rangefinder gives highly accurate measurements of distance. The instrument (lower right corner) is pointed towards a reflective surface (e.g. a face, as shown here) and the reflection of the laser beam provides measurements of direct, horizontal and vertical distance, as well as azimuth and inclination.

3.2.3 Selby rock mass strength

At localities with exposed bedrock, a Schmidt hammer was used to determine the rock hardness. When the Schmidt hammer is pressed perpendicularly onto a rock surface, a spring-loaded metal piston emits a pulse and receives signals indicating the surface hardness (Fig. 11). This is useful for indicating erosiveness, but also to help determining the actual substrate. The process involved describing different parameters: the Schmidt hammer measurements, the degree of weathering, the width, spacing and orientation of joints and the outflow of ground water (Selby, 1982). Rating these parameters gives individual values that are added together to provide a final Selby

rock mass strength. This final value is found within one of the intervals that represent the different rock strengths, which is either very weak, weak, moderate, strong or very strong. The rock mass strength form can be viewed in Appendix 5.

Fig. 11: Measuring rock mass strength by use of a Schmidt hammer can be useful to determine for example rock type and erosiveness. The instrument is shown in the lower right corner, and the procedure is illustrated on the main photo. By pressing the Schmidt hammer perpendicularly onto a surface, a pulse will emit into the rock, and the reflected signals are interpreted by the device to provide the rock strength value.

3.2.4 Anthropogenic inflictions

Human activity may affect several fluvial properties, thus, making notes of such features was an important part of the field work. Dams were among the major disturbances along the stream. Every observed dam was mapped and described in terms of height, and to what extent they seemed to be affecting the sediment transport. Farmlands may also disturb the natural fluvial environment, and observations were made on irrigational devices that drained the stream. Other observations included roads, bridges, villages and channelized parts of the stream.

3.3 Data processing

The final stage of the study involved calculating and plotting fluvial scaling relationships. Data processing included work in *MATLAB* for extracting additional calculated slope values from

the DEM. *Adobe Photoshop* was used for digitally measuring grain sizes from sediment photos. *ArcGIS* allowed for extracting large-scale valley cross sections and *Adobe Illustrator* was used for visualizing the different datasets. In this section, the procedures of sediment analyses, extracting valley cross sections from the DEM and the plotting of fluvial scaling relationships will be described in more detail.

3.3.1 Sediment analyses

Sediment pictures were digitally processed in *Adobe Photoshop* (CS6) to calculate average grain size at localities with exposed gravel bars. This was done by defining the length of the scale bar in each picture after importing it into the program. After designating the amount of pixels found within the length of the scale bar (15 cm), the program is able to do measurements at the same scale. By defining a grid of 11×11 lines, one gets 100 points at which the grid lines intersect. Hence, by measuring the intermediate (b) and longest (a) axis of each grain at an intersection, a random selection of 100 grain measurements is obtained (Fig. 12). This method is similar to the Wolman point count method, but might somewhat under-estimate the grain sizes as the measured diameter depends on the clast orientation relative to the exposure plane (Whittaker et al., 2010).

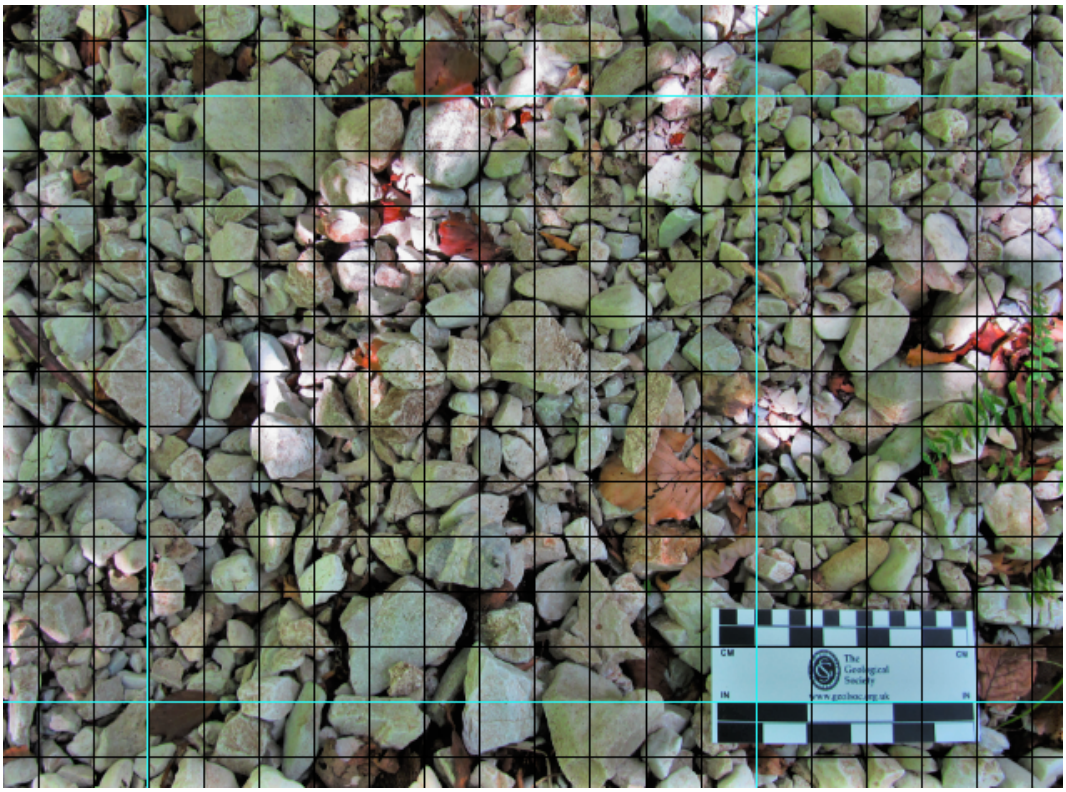

Fig. 12: Sediment pictures with a scale bar were processed digitally to determine average grain size at a certain location. Photos were taken perpendicularly downwards with a visible scale bar, the size of which was digitized in Adobe Photoshop to make grain size measurements. The thin, blue lines represent the outer limits of the grid in which measurements were done at each intersection (photo by A. Geurts).

As all photos were taken perpendicular to the gravel bars, only two of the three axes were visible for each grain. Pebbles usually lie with the shortest axis (c) perpendicular to the surface, therefore only the intermediate and long axes are visible on the sediment photos for measurements. For larger pebbles that covered two or more intersections, measurements were done at each intersection. Where grains were partly covered, an estimation of the grain's extent was needed, and at intersections where the pebbles were covered by for example leaves or the scale bar, no measurements were recorded. Therefore not all sediment photos received a hundred measurements in total. By dividing the intermediate axis by the longest axis, the axial ratio may be calculated. This number can be useful as it has been shown that quantitative information about the transport distance of river pebbles can be extracted by their shape alone (Szabó et al., 2015).

Another important aspect is the grain size distribution at each locality, displayed by plotting the cumulative number (%) of each grain size in what is called a cumulative distribution curve. From this, values of D_{50} (50^{th} percentile) and D_{84} (84^{th} percentile) can be determined. For the D_{50} particle size, 50 % of the grains will be equally-sized or finer than this value. For the D_{84} particle size, 84 % of the grains will be equally-sized or finer than this value. D_{50} represents the median grain size, while the D_{84} is used to describe the coarse fraction of the sediments.

The grain analyses also involved describing the grains in terms of roundness, sphericity and sorting. Sorting was described in general by observing the photos in comparison with the *Chart for visually estimating sorting*, based on Pettijohn et al. (1973) (Fig. 13). Roundness and sphericity, however, could not be determined by a general estimate, but as describing these parameters for all hundred grains on each photo would be excessively time-consuming, ten random grains were described for each photo. This was done by taking a diagonal section from the upper left- to the lower right corner of the measuring grid, describing the grain at each intersection using the roundness chart after Powers (1953) (Fig. 13). The chart rates sphericity into two classes: high and low, while roundness is divided into six classes of very angular, angular, subangular, subrounded, rounded and well rounded. The described grains were given the letter a or b, representing high or low sphericity, respectively, and a value from 1 to 6 representing the roundness classes, where 1 was very angular and 6 was well rounded. The roundness at each locality would then be the mean value of these ten numbers, and the sphericity would be either high or low determined by whether there were most a's or b's.

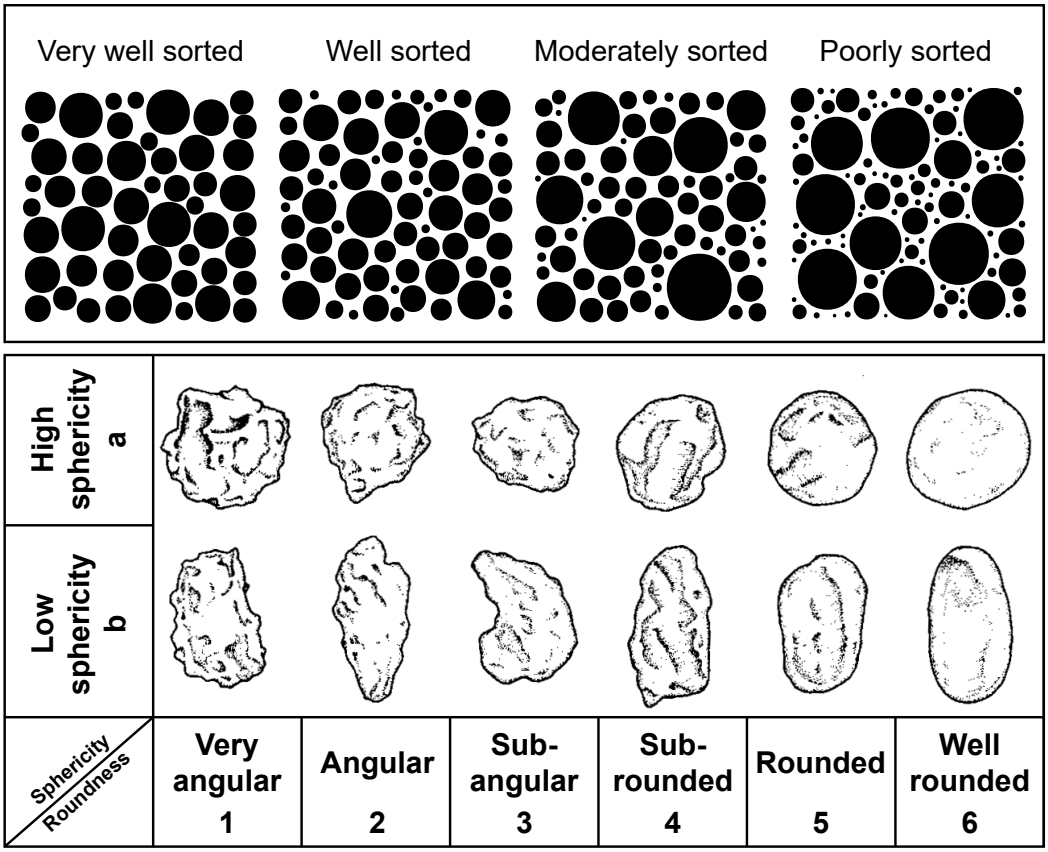

Fig. 13: Upper chart: Chart for visually estimating sorting, modified after Pettijohn et al. (1973). Lower chart: Chart for visually estimating roundness and sphericity, modified after Powers (1953).

3.3.2 Extracting large-scale valley cross sections

ArcGIS was used for extracting large-scale valley cross sections based on the DEM of the catchments. This operation required enabling of the 3D analyst toolbar, and setting the DEM as target layer. The "Interpolate line" tool was then used to draw lines across the river valley at chosen localities that was visited in the field. By clicking the "Create profile graph" tool, ArcMap was able to generate a topography profile for the interpolated line. Generating several profile graphs along the stream made it possible to observe changes in large-scale valley morphology with downstream distance.

3.3.3 Plotting fluvial scaling relationships

The final stage of the data processing was the plotting, calculation and visualisation of the data obtained from field work and computer analyses. Using equations 1-8, these parameters were used to create the resulting plots presented in the next chapter. The following section will explain what choices have been made in terms of what parameters have been used in these calculations and why.

Distance

Most of the measured parameters have been plotted against downstream distance (e.g. Z, A, S, W_b, H_b and USP). Downstream distance can refer either to distance from channel head where the channel starts (dfh) or distance from the drainage divide (dfd). Compared to determining the start of the channel, the drainage divide was easily observed both in the field and on the DEM. Therefore, distance from drainage divide was chosen as the preferred length measurement.

Elevation

Elevation (Z) plotted against downstream distance provides stream long profiles. Three different elevation values were available in this study: the GPS-measurements from the field were taken as close to the channel as possible, often in the active channel itself. However, as the GPS coordinates were imported into ArcMap, the points did not align perfectly with the stream calculated from the DEM. Therefore two other elevation values were extracted digitally from the DEM in addition to these GPS elevations ("Z DEM"): the elevations at the GPS point ("Z DEM locality") and the elevation of the closest point on the stream in the DEM ("Z DEM point"). The resulting elevation plots are combined in Fig. 14, along with a concept figure of how the values were collected. "Z GPS" values were usually highest and the "Z DEM point" values were usually the lowest, however all three values coincided quite well, with a mean difference between the highest and lowest elevations of 7.8 m. The elevations chosen to be used in further calculations were the "Z DEM point" values, as the DEM is considered a key element in this study and the GPS often had large error margins within the narrow reaches of the valley.

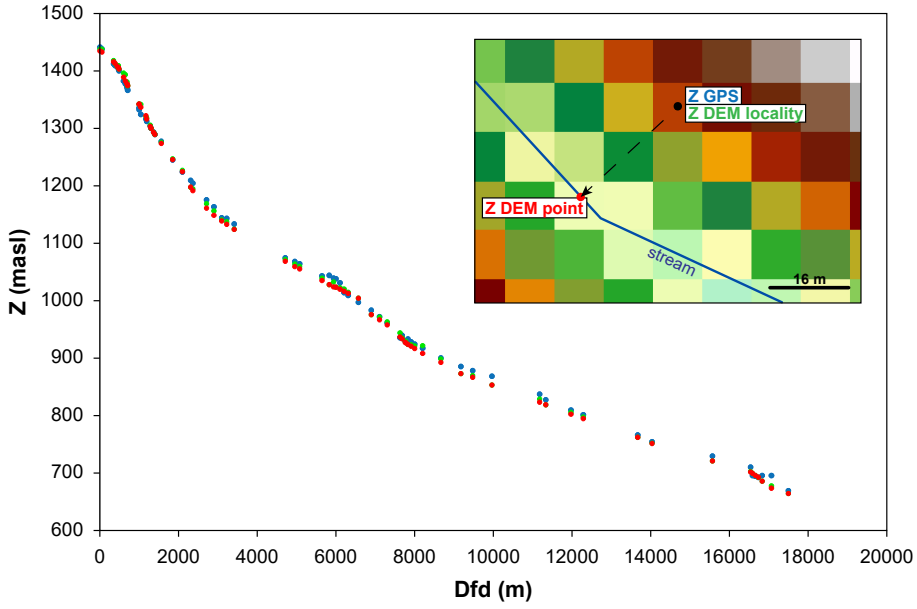

Fig. 14: The plotted elevation values show little variation and display the same overall pattern. The GPS elevation values (blue) were generally the highest, while elevations measured on the stream of the DEM (red) were mostly the lowest. The "Z DEM point" values were chosen to be used as elevation reference further in the study.

Area

Several fluvial models scale with drainage area (A) . Drainage area was calculated from the DEM by first placing pour points at each visited locality along the stream. The pour points, along with the flow direction raster, was used as input it the 'Watershed' tool, which creates a shapefile of the area draining into that specific point on the stream. The procedure was repeated for each locality, after which the drainage area values could be found in the attribute table. Area values were plotted against channel length (eq. 5), width (eq. 6) and slope (eq. 8) to provide the scaling exponents of these different parameters, but was also used in calculating USP (eq. 4).

Slope

Measuring slope (S) with the laser rangefinder in the field was challenging in a stream running through areas of dense vegetation, and the collected values often appeared to be highly local. Therefore, slope values were also calculated from the DEM using MATLAB. The field values and calculated values for Paganica proved to coincide quite well, but as there was a much higher resolution of calculated slope values, this dataset more sufficiently described the whole stream. The calculated slope values were therefore used in further calculations in this study. Slope values were used in calculations of shear stress (eq. 2), Shields stress (eq. 3) and USP (eq. 4), but also in scaling relationships with area (eq. 8) and aspect ratio.

Bankfull channel width and depth

Values of bankfull channel width and depth could only be measured directly in the field, as the DEM resolution of 10 m could not account for the narrow streams in the Paganica and Barete catchments. W_b and H_b were used in calculating hydraulic radius (eq. 1), which is used further when calculating shear stress (eq. 2) and Shields stress (eq. 3). For calculating the USP (eq. 4), the approximate mean value of W_b was used to get a higher resolution of USP values from the entire stream. W_b was also plotted against drainage area to provide the channel width scaling exponent (eq. 6).

4 Results

This chapter is divided into two main parts, presenting the results from field work and data processing for the Paganica and Barete catchments, separately. The final section contains a brief summary of the key observations. The complete datasets for both catchments may be viewed in Appendix 1 (Paganica) and 2 (Barete).

4.1 The Paganica Catchment

4.1.1 Field observations

The Paganica Stream appears to be a mixed alluvial–bedrock river. Near the drainage divide of the Paganica Catchment, the valley is quite flat with rolling hills to the south and the steep Gran Sasso Mountains to the north. The channel is first observed 600 m from the divide as narrow and dry, but likely to contain water in the winter season. The channel contains very angular gravel from the surrounding hillsides, which seems likely to be moved seasonally. Within the first kilometres of the stream, bedrock incision and channel steepening is observed (Fig. 15A), along with a small gorge. Further downstream the channel is steadily widening and deepening.

Water is first observed in the channel about 3.5 km downstream, presumably coming from a side stream and at least one spring. The amount of sediment in the stream fluctuates greatly here, but the grain roundness is clearly increasing. At several localities downstream, large amounts of sediment is added to the channel from scree cones along steep hillsides (Fig. 15B). Most of this is rapidly deposited, resulting in large 'sediment plains' after which the channel contains limited amounts of sediment. Several dams are observed from the headwaters and further downstream. 9 km downstream the stream runs through flat, agricultural areas, where water is clearly being removed, or redirected by various irrigational devices. The slopes in these areas are very low, the stream seems to be shallowing and transporting less water, and active gravel bars are scarce.

From the farmlands and further downstream, the stream runs along the main road, through the villages Assergi and Camarda, where channel width, depth and slope remain more or less constant. At 15 km downstream, however, the valley narrows into a deep gorge with steep valley sides (Fig. 15C). 2 km further down the valley widens again, and the stream continues onto the plain through the town of Paganica where it is channelized in concrete (Fig. 15D). As all natural features of the channel had been erased, no measurements were made beyond this point.

Fig. 15: Selected photos from the field work in the Paganica Catchment. **A:** The upstream reaches of the stream had steep slopes, and bedrock incision was observed at several localities. Dams were observed along the stream, and the photo shows two of the larger ones ($\sim 1.5 - 2$ m) (photo by A. Geurts). **B:** Along the intermediate reaches of the stream, sediment was observed to be added to the channel from large scree cones. The photo is a good representation of the channel dimensions that were observed more or less continuously throughout the stream. **C:** The deep and narrow gorge upstream of the Paganica Fault creates a bottle-neck effect for the stream. This is further enhanced by the main road and the chapel that has been built into the limestone in the narrowest part of the gorge (photo by A. Geurts). **D:** Just downstream of the gorge and the Paganica Fault, the valley widened as the stream continued onto the flat plain in the town of Paganica. From here on the stream was channellized in concrete.

4.1.2 Distance plots

Elevation

A longprofile (elevation against downstream distance) for the Paganica Stream is shown in Fig. 16A. The highest elevation is found at the drainage divide at 1467 masl. The elevation rapidly descends the first 4 km downstream, and then smoothly decrease toward the confluence, where the lowest elevation is found at 584 masl. The longprofile is quite smooth and in lack of major convexities or concavities. Still, three knickpoints may be recognized at approximately 1, 7 and 17 km downstream. The first coincides with observations of steep reaches and bedrock incision in the field. This, however, is very common in headwater reaches of mountain rivers, and needs no further explanation. At 7 km downstream we observed a few rapids and some bedrock incision,

but not as prominent as further upstream. A change in bedrock from limestone to alluvium is found between 8.5 and 9 km downstream on both lithological maps. Finally, the small convexity at 17 km downstream coincides with the gorge that was observed just upstream of the Paganica Fault (Fig. 15C). Here, both lithological maps show a change from limestone to alluvium.

Area

Plot 16B features the change in drainage area with downstream distance, calculated from the DEM. Drainage area is steadily increasing to 40 km^2 during the first 11 km downstream, and then abruptly rises to the double. Another leap occurs at 16 km downstream, after which the area gently rises toward the confluence point to a maximum of 112 km^2. These leaps in drainage area coincide perfectly with the locations at which major side streams enter the channel (Fig. 9); hence the drainage area may suddenly double in size. Because of this effect, caution is needed when plotting other parameters against drainage area.

Slope

The slope plot (Fig. 16C) generally shows little variation with downstream distance. With very few exceptions, the slope values stay between 0 and 0.2 m/m (0 - 10°) throughout the stream. The first 2 km contain a leap from 0.04 m/m (2°) up to 0.83 m/m (47°) and a rapid descent to about 0.1 m/m (6°). These high values coincide with field observations of steep slopes and bedrock incision, common in the headwater reaches of mountain streams. Further downstream, the plot displays a gradually decreasing trend towards the active fault, except for a sudden increase to 0.15 m/m (9°) after 17 km downstream. This easily compares to our field observations of the flat farmland areas in the intermediate reaches of the stream, followed by the narrow gorge upstream of the Paganica Fault.

Bankfull channel width (W_b)

The bankfull channel width dataset (Fig. 16D) is profoundly scattered with hardly any visible trend, except for an initial increase the first 4 kilometres downstream. The values vary between 1.5 and 14 m, with a mean of about 5.6 m. The mean range of error for the W_b measurements were ±0.78 m. An approximate mean channel width of 5 m was used in further USP calculations.

Bankfull channel depth (H_b)

Similar to the channel width, the bankfull channel depth provides a plot (Fig. 16E) displaying a slight increasing trend the first 4 kilometres, followed by scattered values with no visible trend. The channel depths vary between 0 and 2 m, with a mean depth of about 0.8 m. The mean range of error for the H_b measurements were ca. ±0.26 m.

Unit stream power (USP)

The unit stream power calculation (Fig. 16F) uses the approximate mean value of W_b (5 m) for both studied streams. For Paganica, this has resulted in a plot with a definite downstream-rising trend. The first 4 km, the stream power has values up to 0.1×10^6 W/m^2, with a few exceptions of 0.16 and 0.28×10^6 W/m^2. Further downstream, values are scattered between 0.1 and 0.9×10^6 W/m^2, with peak values before the active Paganica Fault from 17 to 18 km downstream. However, this does not reflect what was observed in the field: as water was clearly being removed from the channel within the intermediate reaches, the stream capacity seemed to decrease and stabilize over the downstream half of the stream length, rather than increase as the plot suggests.

Hydraulic radius (R_h)

The hydraulic radius plot (Fig. 16G) shows a slightly increasing trend with downstream distance to the power of 0.4. Values vary between 0.06 m and 1.11 m, with a mean hydraulic radius of ca. 0.6 m.

Shear stress (τ_b)

The overall pattern of the shear stress plot (Fig. 16H) show a decreasing trend, though the values are profoundly scattered. Except for three peaks, the shear stress values are mainly scattered between 0 and 300 kg/m^{2}s^2, and the mean shear stress is 254 kg/m^{2}s^2. The values rapidly increase within the first 4 km downstream, up to the first peak of 785 kg/m^{2}s^2, which roughly coincides with the first observation of continuous flow of water in the channel. This is followed by a drop to less than 300 kg/m^{2}s^2 shortly after. Another peak is reached at about 8.5 km downstream, though values are highly scattered in this area. Between 10 and 17 km downstream, the shear stress seems to be slightly increasing, before a final leap to 815 kg/m^{2}s^2 around 17 km downtream, in the narrowest part of the gorge. The decreasing trend of the shear stress plot reflects what was observed in the field, which was a stream losing water to irrigation, and thereby, power.

Shields stress (τ*)

The Shields stress (Fig. 16I) was calculated using both D_{50} and D_{84} values (Fig. 19A), resulting in two plots that both display a downstream decreasing trend towards the active fault, except for a sudden increase for the last datapoint just upstream of the Pagaica Fault. This decrease, similar to the shear stress plot, coincides with the field observations of water being removed from stream. The plot calculated by using D_{50} values have the highest values ranging from 0.25 to 2.66, with a mean of 0.89. The plot based on D_{84} values range from 0.12 to 1.31, with a mean value of 0.45. Still, the two plots seem to coincide quite well, and both stay well above the threshold value (0.06) for shear stress in transport-limited rivers (Whittaker et al., 2007b, and references therein).

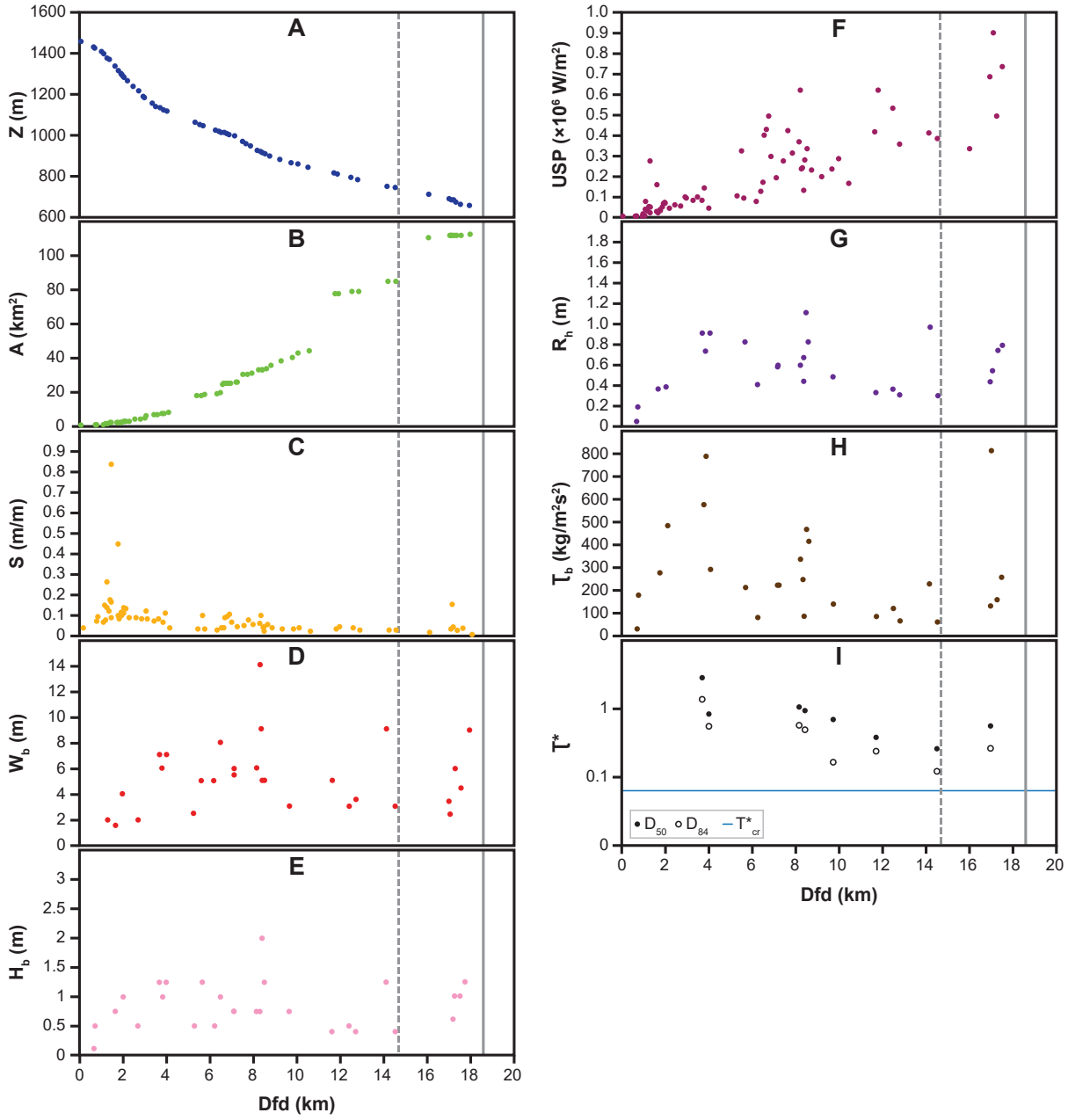

Fig. 16: Field measured and calculated parameters plotted against distance from the drainage divide (dfd). The two faults that the stream intersects are indicated by the grey lines, where the active Paganica Fault is the solid line. **A:** Elevation (longprofile). **B:** Drainage area. **C:** Slope. **D:** Bankfull channel width. **E:** Bankfull channel depth. **F:** Unit stream power. **G:** Hydraulic radius. **H:** Shear stress. **I:** Shields stress using values of both D_{50} and D_{84}, with a thin, blue line indicating the threshold value for critical shear stress in transport-limited rivers.

4.1.3 Area plots

Hack's law

The Hack's law plot (Fig. 17A) displays a log-log plot of how drainage area scales to downstream distance. For Paganica, all datapoints are near perfectly aligned, producing a strongly linear

power trend line with an R^2 value of 0.99 and a Hack's constant h = 0.59. This is remarkably close to the ideal value of 0.6 for a river in dynamic equilibrium (i.e. topographic steady state).

Bankfull channel width (W_b)

Scaling bankfull channel width with drainage area (Fig. 17B) provides a log-log plot of scattered values, leading to the low R^2 value of 0.09. This is consistent with our field observations, where channel widths did not vary greatly downstream. Still, there is an increasing trend, indicating that the channel might be somewhat widening with increasing drainage area. The resulting α = 0.13 is quite low compared to the value for a river in equilibrium where we expect that $\alpha = 0.5$.

Concavity

The slope plot (Fig. 17C) displays a decreasing trend with increasing drainage area. The values are scattered between 0.01 and 1 m/m, giving the R^2 value = 0.33. The resulting concavity index of θ = -0.24 indicates that the slope is indeed decreasing with drainage area, but not with as much as expected for a stream in equilibrium where the θ= -0.5.

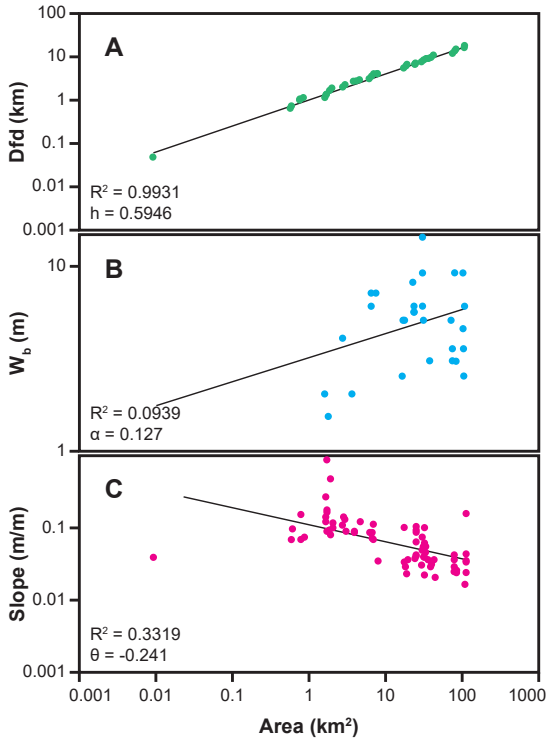

Fig. 17: Field measured and calculated parameters plotted against increasing drainage area. **A:** Distance versus drainage area provides a strongly linear Hack's law plot. **B:** Bankfull channel width versus drainage area provides the channel width scaling relationship, which is profoundly scattered. **C:** Slope versus drainage area provides the concavity index, which for Paganica is shallower than what would be expected for a river in equilibrium.

4.1.4 Aspect ratio versus slope

Aspect ratio versus slope (Fig. 18) seems to be a strongly nonlinear function of slope, although the R^2 value is low (0.23). The steepest slopes (>0.05) are mainly associated with $W_b/H_b <$ 6, which is observed in and after the small gorge at 1.6 km downstream, at 8.5 km downstream where the stream incises into bedrock at several localities, and at 17 km downstream in the deep gorge upstream of the Paganica Fault. Lower slopes (<0.05) are mainly associated with W_b/H_b > 6, which is observed over large parts of the stream length where there are wide and shallow channels.

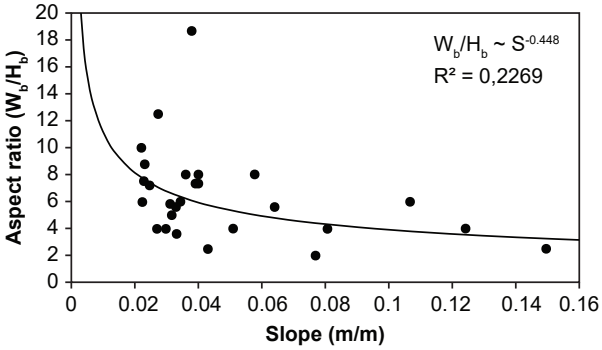

Fig. 18: The aspect ratio versus slope correlation provides insight in how a channel changes shape with changes in slope. For the Paganica Catchment, this relationship is observed to be strongly non-linear, despite the poor fit of the trend line.

4.1.5 Grain analyses

The Paganica Catchment contained numerous gravel bars with grains of solid limestone. Most of these were located upstream of the farmland areas, between ca. 2 and 9 km downstream, were sediment at times filled the entire valley floor. Within the farmland areas and further downstream, sediment volumes decreased and much of the bedload was at times dominated by sand. Nine gravel bar localities were chosen to represent the grain analyses: three from the upstream reaches, three from the intermediate section (farmland areas) and three from the downstream reaches. This is shown in Fig. 19 (complete description of the grain photos are gathered in Appendix 5). Plot 19A displays the values of the median and coarse grain fractions at each locality. The D_{84} values are more scattered than the D_{50} values, particularly in the intermediate part of the stream, and vary from 25 to 62 mm. The more stable D_{50} values vary between 13 and 32 mm. Hardly any trend is visible from the resulting plot, but there might be a slight increase in the intermediate section, and a slight decrease further downstream. The mean axial ratios (plot 19B) all remain within 0.6 and 0.7. The mean roundness (plot 19C), however, show a definite change from angular/sub-angular in the upstream areas, to sub-rounded/rounded further downstream. This was also observed in the field, illustrated in Fig. 20 with photos of gravel bars from the upstream and downstream reaches.

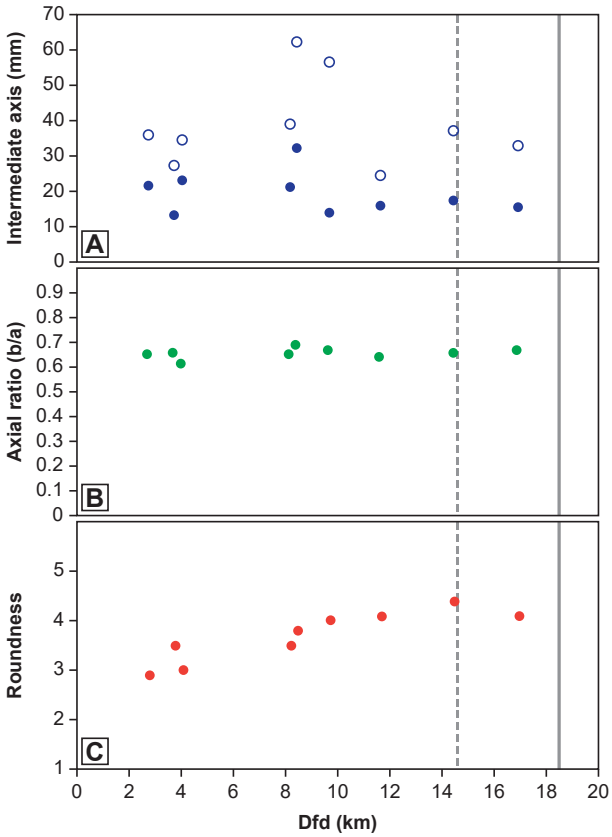

Fig. 19: Results of the grain measurement analyses, with the Assergi and Paganica faults indicated by dashed and solid grey lines, respectively. **A:** Size of the intermediate grain axes in mm, represented by D_{50} (filled dots) and D_{84} (empty dots). The elevated D_{84} values in the intermediate reaches of the stream stand out compared to the more stable D_{50} values. **B:** Axial ratio (b/a) remains more or less constant throughout the stream. **C:** Average grain roundness, determined visually by comparison with the chart after Powers (1953), show a definite downstream increase in roundness. The y-axis in this plot is based on the values on the lower chart in Fig. 13.

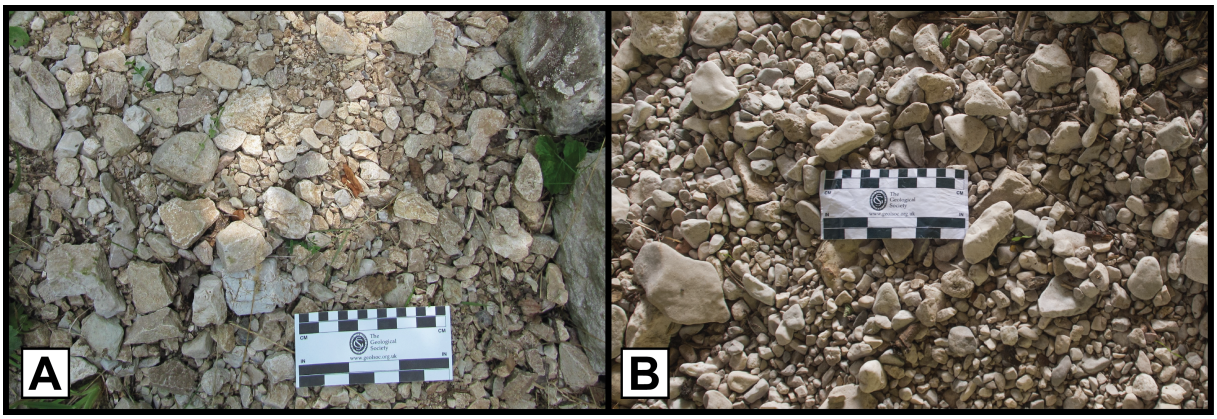

Fig. 20: The gravel bars in the Paganica Catchment contain limestone grains that visibly increase in terms of roundness with downstream distance. **A:** In the upstream reaches (1.7 km downstream) the limestone gravels are mainly angular to subangular (photo by A. Geurts). **B:** Further downstream (14.5 km downstream) the grains are subrounded to rounded.

Cumulative frequency curves were plotted for all nine localities, and combined in one plot (Fig. 21). This shows that the cumulative distributions of the intermediate grain size are quite similar at all localities, especially at and below the D_{50} values. Above the coarser percentiles, however, the frequency curves become much more scattered towards coarser grain sizes, to a maximum of 12 cm. The intermediate section of the stream stands out as far more skewed compared to the other frequency curves. This indicates that the intermediate reaches of the stream contains more coarse sediment than the upstream and downstream areas.

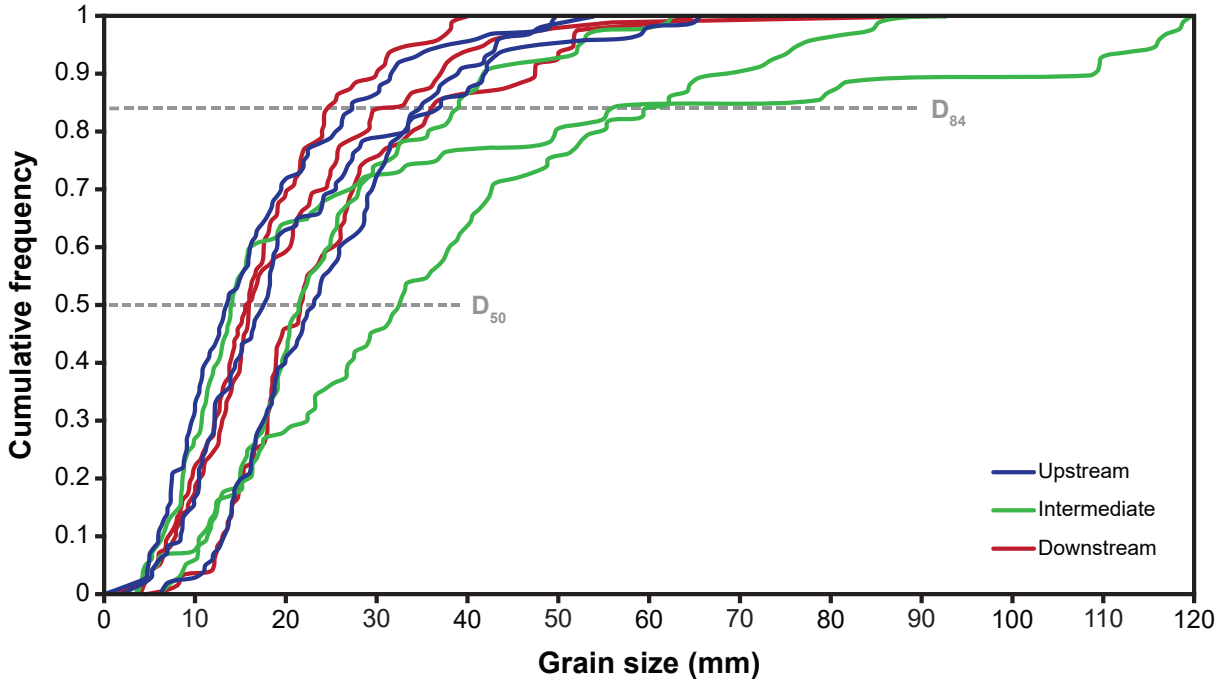

Fig. 21: Cumulative frequency curves for all nine grain analysis sample localities. The distributions are quite similar for all localities, particularly below D_{50}. Above the coarse grain percentile (D_{84}), however, there is a much higher amount of scatter to coarser grain sizes. The frequency curves for localities within the intermediate section of the stream (green) is much more skewed compared to the upstream (blue) and downstream (red) sections of the stream.

4.1.6 Valley cross sections

Ten valley cross sections were extracted from the Paganica Catchment (Fig. 22). The valley starts as quite a narrow feature, and narrows even more further downstream. From profiles 3–6, the valley is generally widening and flattening, but from profile 7–9, the valley narrows as the gorge is approached. There, the profiles acquire a smooth, M-like shape. At the Paganica Fault, downstream of the deep gorge, the valley again widens and disappears altogether as the flat areas around the town of Paganica are reached.

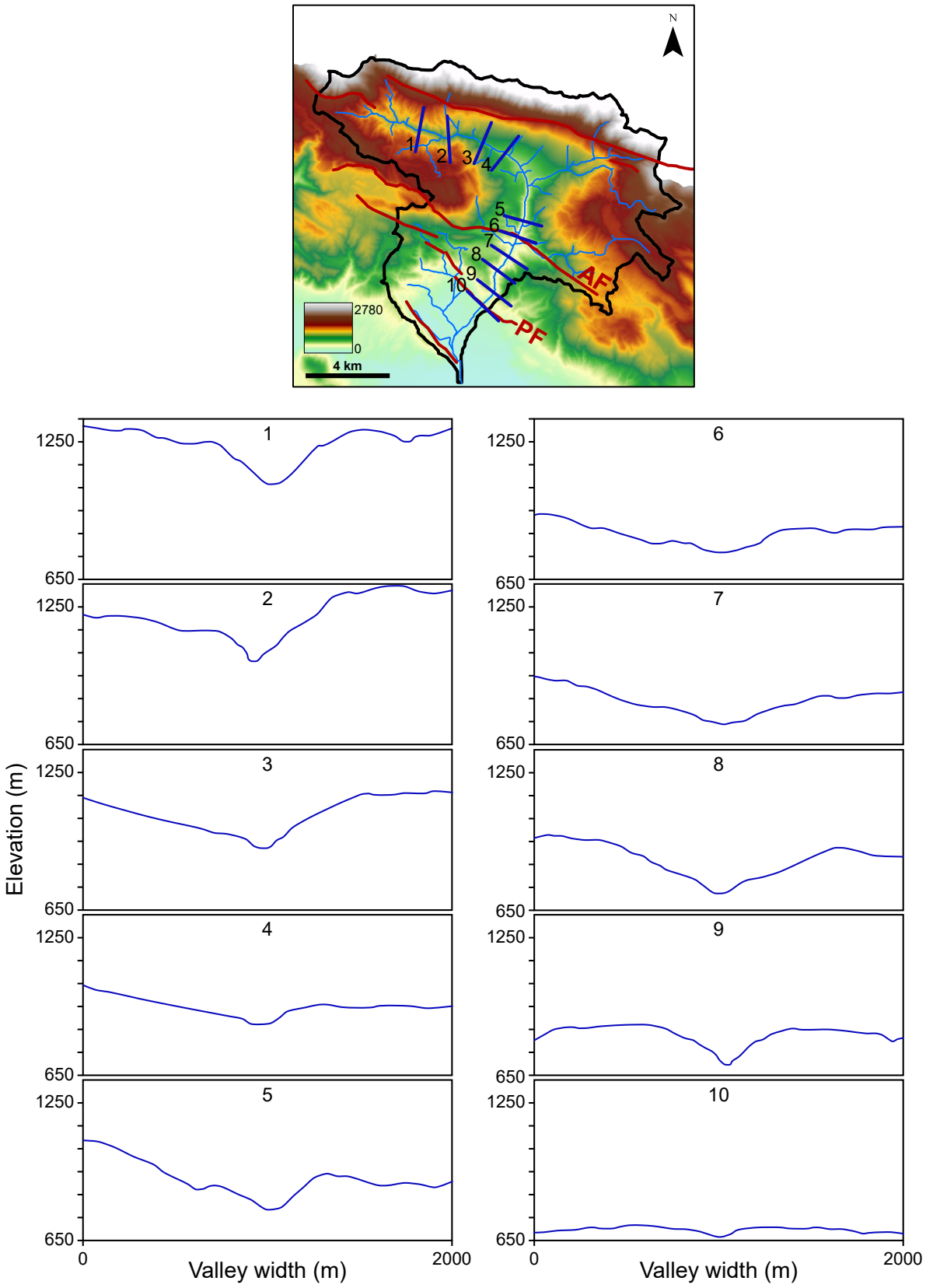

Fig. 22: Valley cross sections extracted from the DEM (Tarquini et al., 2012) for the Paganica Catchment. All profiles are drawn as looking downstream, and all have a cross-sectional width of 2 km and an elevation range of 700 m. In the headwaters of the Paganica Stream, the valley is quite narrow, while the intermediate reaches display more gentle valley profiles. Upstream of the confluence, the valley is observed to narrow and deepen progressively closer to the Paganica Fault (PF).

4.2 The Barete Catchment

In the headwaters of the Barete Catchment, the channel was difficult to reach, and so there is a lack of data upstream of the Montereale Fault. Also, due to the lack of well-developed, accessible gravel bars, there is no grain analysis dataset available for the Barete Catchment. The sediment descriptions are therefore not as detailed as for Paganica, and Shields stress has not been calculated because of the lack of D_{50} and D_{84} values.

4.2.1 Field observations

The Barete Stream also have characteristics of both alluvial and bedrock rivers, but with seemingly less sediment than Paganica. Close to the drainage divide, the Barete Catchment is bordered by moderately steep hillsides. The dry and narrow channel moves through a wide and elongated valley with progressively steepening hills on both sides (Fig. 23A). Between 4 and 5 km downstream, a distinct knickpoint is observed where the valley deepens and narrows and contains several reaches of steep bedrock incision (Fig. 23B). This is also where the stream may be intersecting the tip of the Montereale Fault. Small pools of water are observed along steps in the channel, but these disappear shortly after.

Downstream of the knickpoint there is little variation in bankfull width and depth, and the channel is at times difficult to follow. A few large dams are observed. Gravel bars are observed sporadically, but just upstream of the village of Capitignano, longer reaches of the channel are continuously filled with sediment. After 7 km downstream the slope decreases as the channel reaches the flat farmland areas near the village of Capitignano (Fig. 23C). Here, parts of the channel is built in with concrete and contains very well rounded gravel. Past the village Capitignano, the stream runs close to the main road where it is no longer channelized and contains running water (Fig. 23D). Channel widths and depths increase, as is the water and sediment yield. In the village of Marano, the stream intersects the Barete Fault and continues as the Aterno River.

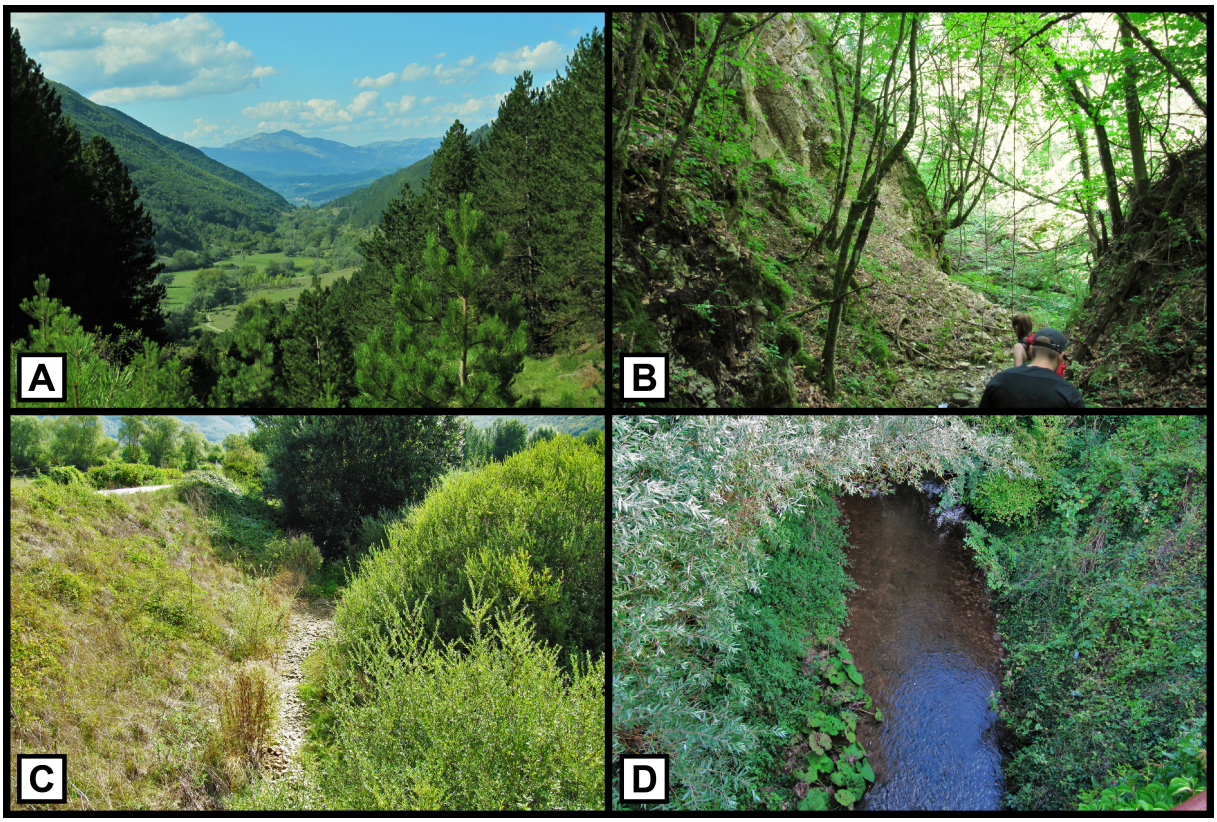

Fig. 23: Selected photos from the field work in the Barete Catchment. All photos by A. Geurts. **A:** The headwater reaches of the stream had gentle slopes bounded by steeper hillsides. The channel was very narrow and dry. **B:** Within the convex reaches of the stream the valley was quite narrow with steep hillsides and bedrock incision. The actual channel was at times difficult to follow in the dense vegetation. **C:** Within the flat farmland area the channel was narrow and dry, but with well rounded gravel, indicating that water is occationally transporting the sediment. **D:** Downstream of the Paganica Fault the channel was wider and deeper, filled with gently flowing water and coarse sediment.

4.2.2 Distance plots

Elevation

The Barete longprofile (Fig. 24A) show rapidly decreasing elevations from >1400 m to 1200 m the first kilometre, followed by a flat reach until 4 km downstream. Then, a pronounced knickpoint with an elevation difference surpassing 200 m is observed between 4.5 and 9 km from the drainage divide, close to where the Montereale Fault may be intersected by the stream. After the knickpoint, the elevations make up a graded profile for the rest of the stream length, to below 800 m. This clearly reflects what was observed in the field: a gently sloping headwater area, a steep knickzone with bedrock incision in the intermediate reaches, followed by more or less flat farmlands further downstream.

Area

The area plot (Fig. 24B) features a steady increase up to 25 km^2 during the first 11 km downstream. Then follows a leap to 66 km^2, after which there is a steady increase up to 79 km^2 near the Barete Fault and the confluence. Between 11 and 12 km downstream, two side-streams enter the channel: first a minor side-stream from the southeast, followed by a major side-stream from the north, explaining this sudden leap in drainage area.

Slope

Plot 24C displays the MATLAB-calculated values of slope for the Barete Catchment. The plot generally shows little variation in slope with downstream distance, with values varying from 0 to 0.26 m/m (0-15°) throughout the stream. Peak slope values are found within the first half of the stream length, the highest one at the drainage divide where S = 0.26 m/m (15°). There may also be a small peak near the Montereale Fault. Further downstream, the slope steadily decreases to a minimum of 0.0027 m/m (0.15°) at 12 km downstream. Approaching the Barete Fault, slope increases to 0.03 m/m (1.8°), before a drop to 0 m/m near the Barete Fault.

Bankfull channel width (W_b)

The bankfull channel width dataset (Fig. 24D) consists of scattered values between 1 and 9 m, with a mean value of approximately 5.4 m. It is difficult to determine any visible trend the first 12 km downstream, where the values fluctuate around 4 m. However, there seems to be an increasing trend towards the Barete Fault, as the three highest values of W_b (9 m) are all found within the last 2 km of the stream length.

Bankfull channel depth (H_b)

Bankfull channel depth (Fig. 24E) follows the pattern of the W_b plot, with similar values the first 12 km downstream, followed by peak values near the Barete Fault. Values are scattered between 0.5 and 3 m, with a mean value of 1.2 m. The first 12 km, channel depth varies from 0.5 to 1 m, but after 15 km downstream the channel deepens to 2.25 m, and reaches the maximum depth of 3 m at the Barete Fault.

Unit stream power (USP)

The unit stream power plot (Fig. 24F) for the Barete Catchment have values scattered mainly between 0 and 0.2×10^6 W/m^2, but there seems to be two clear peaks. Due to the lack of field data from the upstream reaches of the catchment it is impossible to see the development of USP upstream of the Montereale Fault, but there is surely some sort of increase from the drainage divide up to 0.24×10^6 W/m^2 at 5.5 km downstream. The stream power then gently decreases

until about 10 km downstream, before another increase towards the Barete Fault, to a peak of almost 5×10^5 W/m^2. This mainly reflects what was observed in the field: steep upstream reaches followed by very low slopes, and then slightly higher slopes and a channel filled with flowing water.

Hydraulic radius ($\mathbf{R_h}$)

The hydraulic radius (Fig. 24G) is more or less stable between 5 and 12 km downstream, with values varying from 0.38 m to 0.75 m. This is followed by an abrupt increase to 1.5 m, and finally, 1.8 m near the confluence.

Shear stress (τ_b)

For Barete, the first shear stress (Fig. 24H) value is found at 5.3 km downstream, close to where the stream may be intersecting the Montereale Fault, where τ_b= 58 kg/m^{2}s^2. This is followed by a drastic increase to 534 kg/m^{2}s^2 a few hundred metres further downstream. Less than a kilometre further downstream, the shear stress drops to below 200 kg/m^{2}s^2, and reaches the minimum value of 11 kg/m^{2}s^2 at 12 km downstream. A final increase in shear stress provides a value of 248 kg/m^{2}s^2 at the Barete Fault. The mean shear stress throughout the stream is 180 kg/m^{2}s^2.

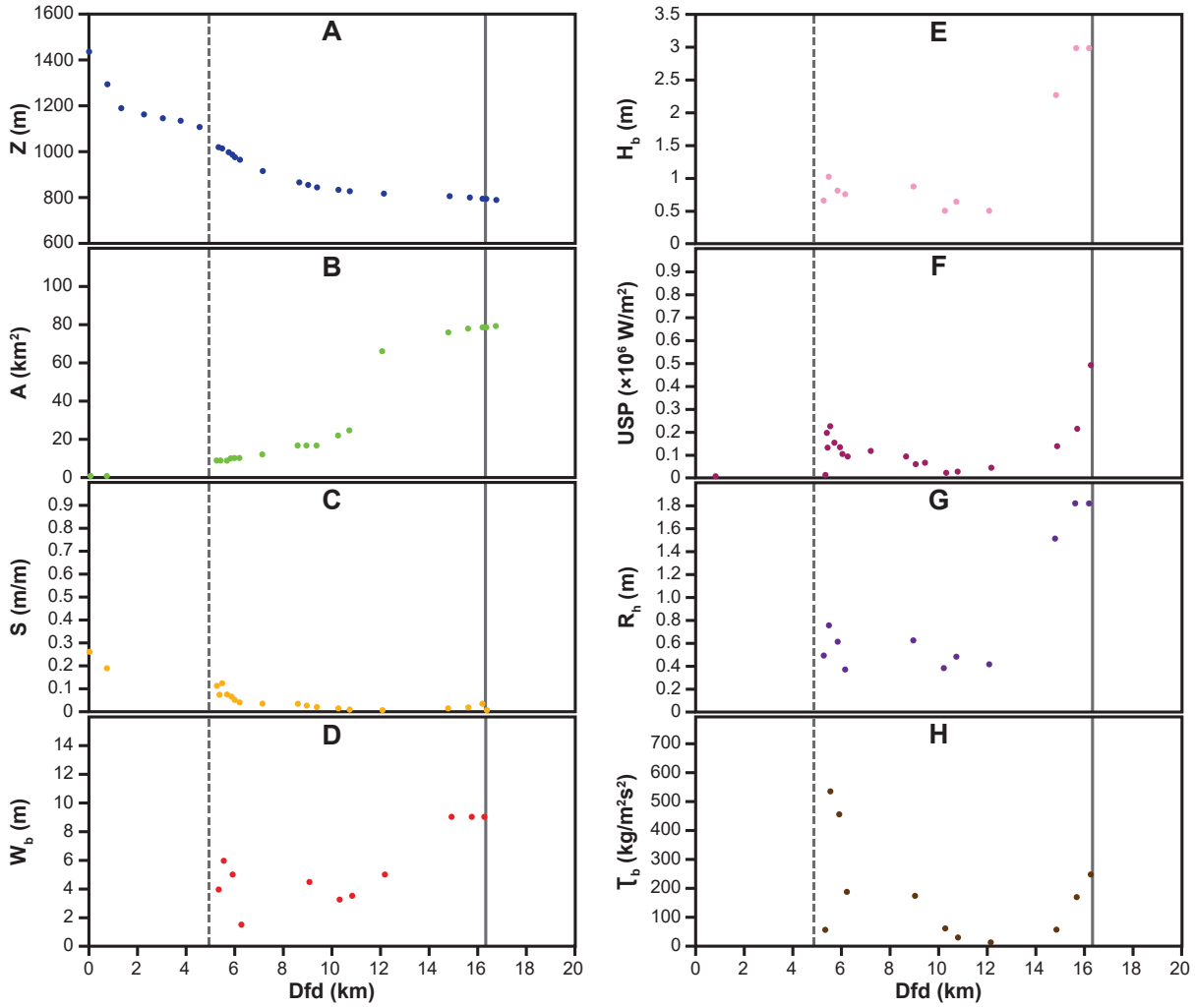

Fig. 24: Field measured and calculated parameters plotted against downstream distance, with the Montereale Fault marked with a dashed line and the Barete Fault marked as a solid grey line. **A:** Elevation (longprofile). Because of the lack of field measurements in the upstream reaches of the Barete Catchment, the five elevation values between 1.3 and 4.5 km were extracted from the DEM to fill the gap. This was done for visual purposes only, to show the knickpoint. **B:** Drainage area. **C:** Slope. **D:** Bankfull channel width. **E:** Bankfull channel depth. **F:** Unit stream power. **G:** Hydraulic radius. **H:** Shear stress.

4.2.3 Area plots

Hack's law

The Hack's law plot (Fig. 25A) for Barete displays an almost perfectly linear power trend line with an R^2-value of 0.97. The resulting Hack's constant (h = 0.53) is lower than the value for a river in equilibrium (h = 0.6), but still quite close.

Bankfull channel width (W_b)

Channel width versus drainage area provides a log-log plot (Fig. 25B) of scattered values, leading to the low R^2 value of 0.2. Still, there is a generally increasing trend, indicating that the channel might be somewhat widening with increasing drainage area. This results in $\alpha = 0.15$, which is very low compared to the value for a river in equilibrium ($\alpha = 0.5$).

Slope

The concavity index (Fig. 25C) for the Barete Catchment is steeply plunging with larger drainage area. The R^2 value of 0.7 means a reasonable fit of the trend line, providing a concavity index, θ, of almost -1. This is much higher than the concavity index expected for a stream in equilibrium, where θ should be close to -0.5.

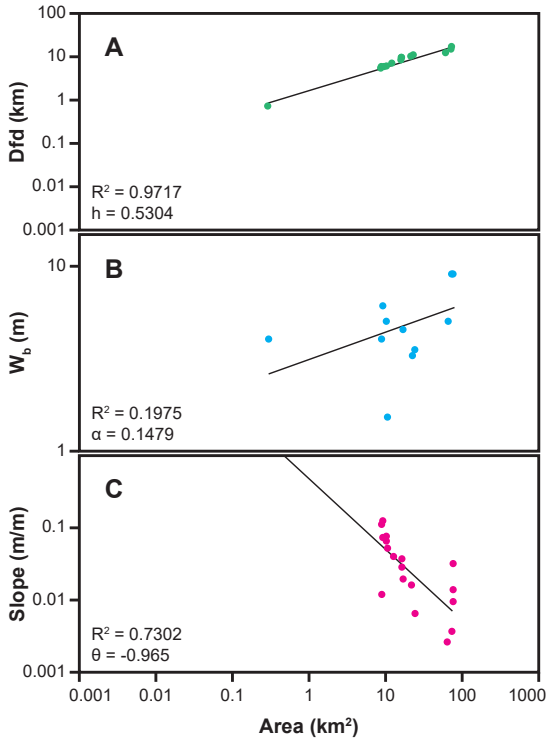

Fig. 25: Field measured and calculated parameters plotted against increasing drainage area. **A:** Distance versus drainage area provides a strongly linear Hack's law plot. **B:** Bankfull channel width versus drainage area provides the channel witdth scaling relationship, which is poorly fit by the trend line. **C:** Slope versus drainage area provides the concavity index, which for Barete is much steeper than what would be expected for a river in equilibrium.

4.2.4 Aspect ratio versus slope

For Barete, aspect ratio versus slope provides a plot with quite few values, and very little variation (Fig. 26). The power trend line has a very poor fit of $R^2 = 0.05$, and the power-law exponent has the low value of -0.089. There is next to no difference between W_b/H_b associated with high slopes (>0.05) and W_b/H_b associated with low slopes (<0.05), and aspect ratio therefore seems to be a more linear function of slope for this stream.

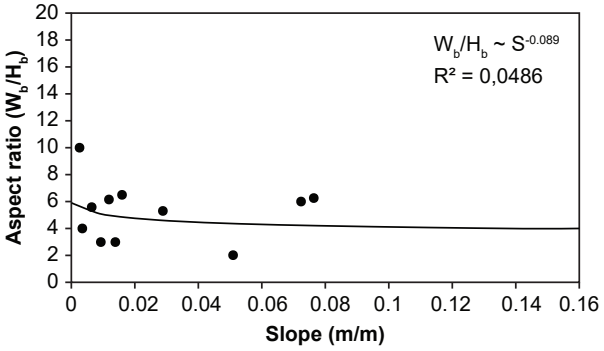

Fig. 26: The aspect ratio versus slope plot for the Barete Stream display more constant aspect ratios with increasing channel slope, although the fit of the trend line is very poor.

4.2.5 Grain analyses

The Barete Catchment had few accessible and well-developed gravel bars compared to Paganica, so only a limited number of sediment photos were taken. In addition to limestone, the gravel bars contained grains of carbonate flysch. The low number of sediment photos is determined to be insufficient for providing a wholesome grain analysis for the stream. In general, the upstream reaches contained poorly sorted gravel bars made up of sub-angular to angular grains. Within the knickzone, large boulders were observed along the valley floor, derived from the steepened hillslopes. In the flat farmlands in the intermediate section of the stream, both sorting and roundness improved greatly, with numerous well rounded grains. However, in the downstream reaches where there was water in the channel, grain sizes were observed to increase again, while the degree of rounding decreased (Fig. 27).

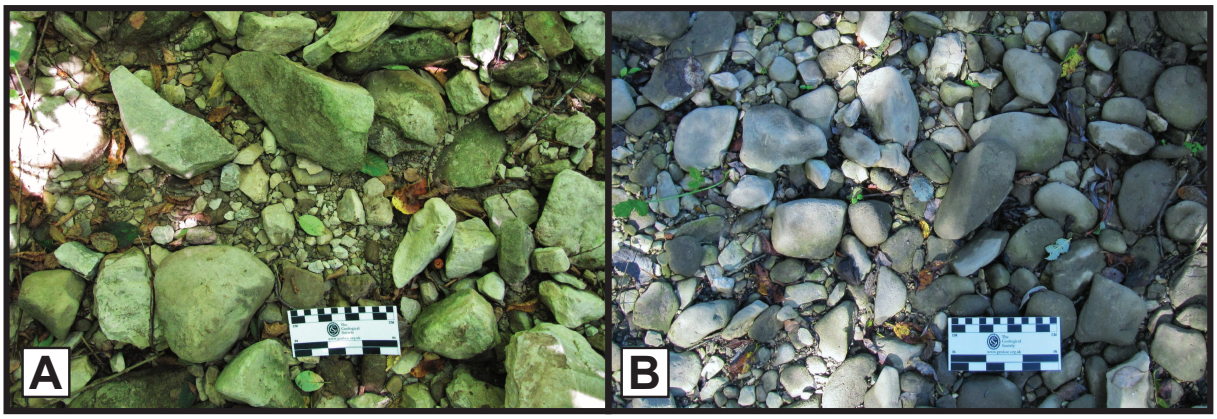

Fig. 27: Gravel bars in the Barete Catchment contained grains of both limestone and flysch. Both photos by A. Geurts. **A:** In the upstream reaches the gravels are mainly subangular. **B:** In the downstream reaches the grains are rounded to well rounded.

4.2.6 Valley cross sections

As the Barete Catchment is smaller, containing a shorter stream, only eight valley cross sections were extracted (Fig. 28). The headwater reaches of the stream does not display a distinct gorge-like feature as in the Paganica Catchment, and the valley is generally wide and shallow. Profile 2, 3 and 4 display the steep hill southwest along the stream, and profile 2 stands out with its distinct V-shape. Between profile 2 and 3 the valley changes from a distinct V-shape to a more gentle profile. The area between these profiles is where we find the knickpoint and the possible intersection with the Montereale Fault. This is also the area where we observed steep reaches and bedrock incision in the field. As the stream continues onto the flat plateau with farmland areas, the cross sections appear almost flat. The most downstream profiles 7 and 8 show that the valley becomes more narrow approaching the Barete Fault.

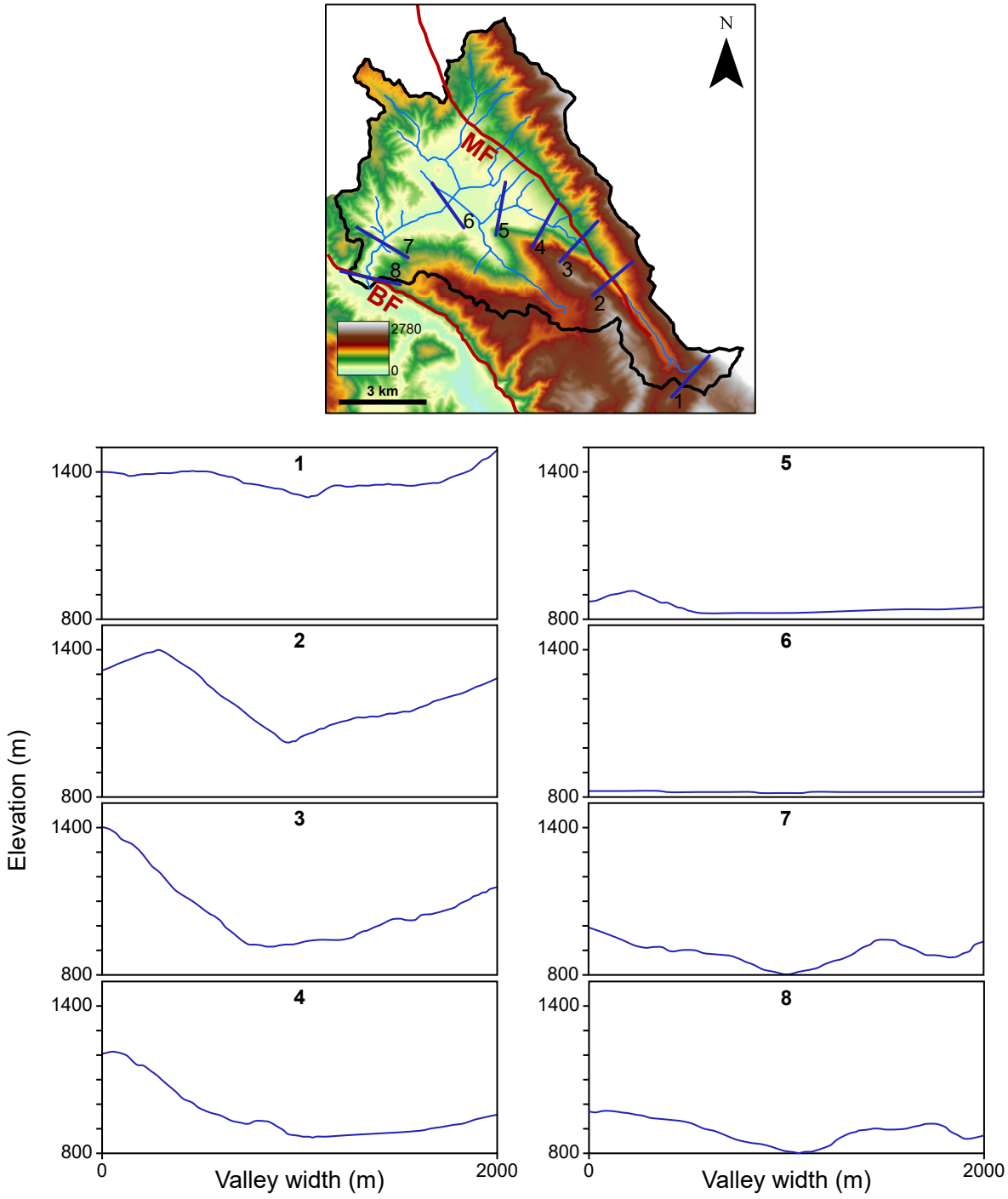

Fig. 28: Valley cross sections extracted from the DEM (Tarquini et al., 2012) for the Barete Catchment. All profiles are drawn as looking downstream and have the cross-sectional width of 2 km. The elevation range is the same as for Paganica (700 m), but between 800–1500 masl instead, as the Barete Catchment has higher average elevations than the Paganica Catchment. The cross-sections show less dramatic downstream changes compared to the Paganica Stream. The valley is observed to narrow closer to the Barete Fault (BF), but no gorge-like feature is observed. The second cross section stands out with the sharp V-shape. This coincides with the observations of steep and narrow valley reaches near the headwaters of the stream, close to the Montereale Fault (MF).

4.3 Summary of results

The results of field work and data processing for both catchments are compiled into the following key observations:

- Both streams contain distinct longprofile convexities (Figs. 16A and 24A).
- Slopes decrease with downstream distance, but increases upstream of the faults Figs. 16C and 24C).
- Bankfull channel width remains more or less constant ($\sim$ 5 m) throughout the Paganica Stream (Fig. 16D), whereas the Barete Stream displays more of a downstream-widening trend (Fig. 24D).
- Bankfull channel depth remains more or less constant throughout the Paganica Stream (Fig. 16E), whereas the Barete Stream displays a downstream-deepening trend (Fig. 24E).
- Unit stream power greatly increases downstream for the Paganica Stream (Fig. 16F), whereas the pattern for Barete is more complex with a weak increase (Fig. 24F).
- Hydraulic radius remains more or less constant throughout the Paganica Stream (Fig. 16G), whereas the Barete Stream displays a downstream-increasing trend (Fig. 24G).
- Shear stress decreases for the Paganica Stream, before a rapid increase upstream of the Paganica Fault (Fig. 16H). For Barete, shear stress decreases downstream of the Montereale Fault and increases slightly upstream of the Barete Fault (Fig. 24H).
- Shields stress for the Paganica Stream follows a downstream decreasing trend, followed by an increase just upstream of the Paganica Fault (Fig. 16I). All values stay well above the threshold for transport-limited rivers.
- Distance versus drainage area provide strongly linear plots for both catchments (R^2>0.9), with Hack's constant h$\simeq$ 0.6 for both streams (Figs. 17A and 25A).
- Channel width versus drainage area provides $\alpha = 0.13$ for Paganica (Fig. 17B) and $\alpha = 0.15$ for Barete (Fig. 25B), which is much lower than what is expected for an equilibrium stream ($\alpha = 0.5$).
- Slope versus drainage area indicates a very high concavity ($\theta = -0.97$) for Barete (Fig. 17C) and a very low concavity ($\theta = -0.24$) for Paganica (Fig. 25C), compared to a river in topographic steady state ($\theta = -0.5$).
- Aspect ratio is a highly non-linear function of channel slope for Paganica (Fig. 18), whereas Barete has a more constant aspect ratio with higher slopes (Fig. 26).
- The Barete Stream seems to contain less sediment than Paganica, but a downstream increase in roundness is evident for both streams (Figs. 20 and 27).

- Sediment analyses for Paganica reveal constant axial ratios and increasing roundness downstream. D_{50} values are quite constant, while the D_{84} values peak in the intermediate reaches of the stream. The cumulative frequency curves show little variation for the lower frequencies and much more variation for the higher frequencies (Fig. 19).

- The valley cross sections show more dramatic changes in valley shape for Paganica (Fig. 22) than for Barete (Fig. 28). Downstream of the Paganica Fault the Paganica Stream widens immediately, while no sudden change is observed for the Barete Stream downstream of the Barete Fault. There is, however, a distinct V-shaped profile near the Montereale Fault in the Barete Catchment.

5 Discussion

The ambition of this study has been to better understand landscape dynamics within the tectonically active Abruzzo Region in central Italy. In order to do this, we set out to investigate the following questions:

- Are the Paganica and Barete catchments in topographic steady state?
- Are these two catchments interacting?
- Would a study of the Paganica Stream have helped us to foresee such an event as the devastating L'Aquila earthquake in 2009?

Whether or not the Barete and Paganica streams are undergoing a transient response to faulting is highly related to the faults they intersect. This chapter therefore starts with reviewing the normal faults found within each catchment. Next, a step by step review of the different factors that could determine whether or not the Barete and Paganica streams are undergoing a transient response to tectonic forcing, is presented. Regarding this matter, a review of Hack's law and its use in identifying transient rivers, is given. The possibility of the two catchments interacting with one another is discussed, before a debate on whether or not a study like this would have been able to help to predict the L'Aquila earthquake. After a discussion of the sources of error for this study, an attempt is made to determine how the results of this study may reflect the overall landscape dynamics of the region.

5.1 The faults

The Paganica and Barete catchments are located about 50 km and 30 km away from the NW edge of the central Apennines fault array, respectively (Roberts and Michetti, 2004). As mentioned in Chapter 2.3, throw and throw-rate maximums are higher for the more central faults (Cowie and Roberts, 2001). Thus, based on this statement, the faults within the Paganica Catchment should be more active than the faults within the Barete Catchment. Another important aspect is where the streams intersect the faults, as fault offsets generally decrease towards the fault tips (e.g. Cowie and Roberts, 2001; Roberts and Michetti, 2004). The Paganica Stream intersects the Assergi Fault and, more importantly, the Paganica Fault in the very centre, whereas the Barete Stream possibly intersects the Montereale Fault and the Barete Fault at the fault tips. Therefore we would expect the Barete Stream to be affected by lower fault slip rates, and thus exhibit less of a transient response than the Paganica Stream.

With the benefit of hindsight, Blumetti et al. (2013) suggested that the listric appearance of the faults within the Paganica Catchment is a sign that they all join the Paganica-San Demetrio fault system at depth. They refer to this fault system as the master fault of the whole Gran Sasso-Middle Aterno Valley fault system, and the main seismic source of the Middle Aterno

Valley basin. They conclude that the Paganica Fault has been – and still is – a major factor in the landscape evolution of the L'Aquila region, despite its minor geomorphic appearance. Based on this, there is little doubt that the Paganica Fault is an active feature that impacts the surrounding area. What is interesting about this is the fact that the Barete Catchment has a larger and more distinct knickpoint, whereas Paganica has three smaller convexities (e.g. Fig. 29). This will be further discussed in section 5.2 (Stream longprofiles).

Whittaker et al. (2007b) indicate that the response timescale to fault acceleration is ~ 1 Myr to re-equilibriate local channel slopes, and < 3 Myr to regain good hydraulic scaling, meaning that transient responses can remain in the landscape for a long time. They estimated that approximately 2 Ma would be required for catchments in the Apennines to achieve steady state. Fault initiation occurred at 3 Ma (Cavinato and De Celles, 1999), and fault acceleration around 0.75 Ma (Roberts and Michetti, 2004), which indicates that both catchments should have been in equilibrium at the time of fault slip acceleration, but may not yet have reequilibrated since then.

5.2 Stream characteristics

Stream longprofiles

For studies concerning mountainous rivers, stream longprofiles provide highly useful information. In areas of rapid erosion and tectonic uplift, longitudinal profiles of bedrock or bedrock-alluvial hybrid channels are better indicators of uplift rate than other morphological properties (Whipple, 2004). Using eq. 7, theoretical longprofiles for the Paganica and Barete streams have been calculated, using constants from the previously mentioned Penaro River, which is in topographic steady state. Thus, we calculate theoretical "equilibrium profiles" for the two streams. Comparing this to the actual profile makes it evident that neither Paganica nor the Barete streams possesses the typical profile shape of an equilibrium river (Fig. 29). Possible explanations for the convexities in both catchments will be reviewed in the following sections.

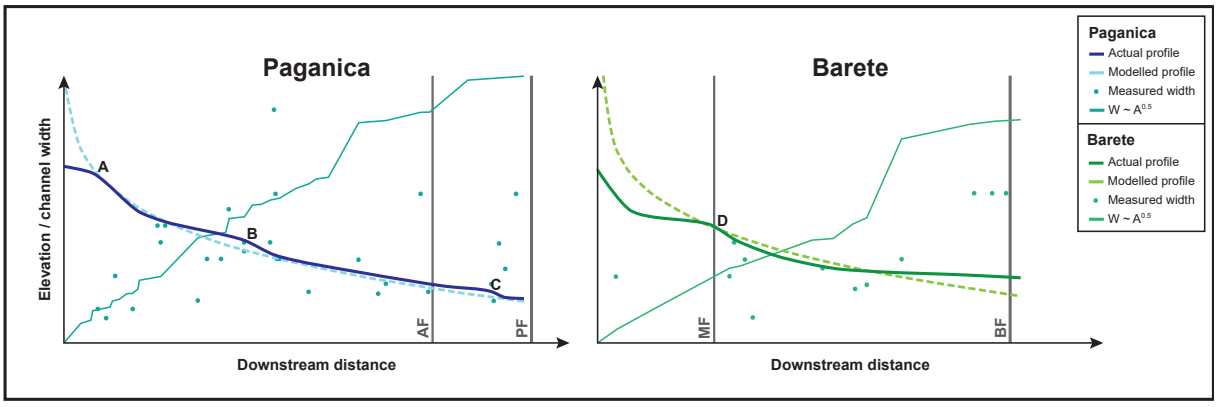

Fig. 29: By using parameter values from a river known to be in equilibrium (the Penaro River), it is possible to model the equilibrium profiles of the Paganica and Barete streams. The calculated profiles enhance the presence of convexities in both streams, making it evident that neither of the streams have the concave-up shape that is typical for rivers in equilibrium. Using the model W$\sim A^{0.5}$, which assumes topographic steady state, expected channel widths for Paganica and Barete have been calculated (using a constant of 0.015). Compared to the measured width values (dots), the model seems to highly overestimate channel width in the downstream reaches of both streams, which indicates a transient response for both Paganica and Barete. Both plots have the same dimensions. Downstream distance = 2 km. Elevation range = 400–2000 masl. Channel width = 0–16 m. MF = Montereale Fault, BF = Barete Fault, AF = Assergi Fault, PF = Paganica Fault.

The Paganica Catchment longprofile

As steep slopes and bedrock incision is a common feature for mountain rivers, knickpoint A (Fig. 29) needs no further explaining. Knickpoint B is located 7 km downstream. The observed change from limestone to alluvium between 8.5 and 9 km (Fig. 2D) indicate that knickpoint B may be lithology related. However, lithology is not synonymous with rock properties: a well consolidated alluvial deposition may be stronger than weathered limestone, and the strength may vary markedly within one unit (Wobus et al., 2006). Nevertheless, this needs to be examined. The ISPRA map (Fig. 2D) show that the stream is barely touching this boundary, whereas in the map from Vezzani and Ghisetti (1998)(Appendix 6), the stream is clearly intersecting the alluvium. However, for both maps there is a distance of >1 km between the knickpoint and the change in lithology, which may be too far to connect the two features, as a lithological knickpoint should appear right on the boundary. Nevertheless, errors in either of the geological maps could mean that the knickpoint is misplaced compared to the lithology, and so this possibility cannot be dismissed completely.

Another explanation for knickpoint B is that it is a transient response to increased slip of the Paganica Fault at $\sim$ 0.75 Ma. This implies that the knickpoint has migrated >10 km within this timespan. Whittaker et al. (2008) showed that field estimates of knickzone propagation rates are a function of fault slip rate as well as drainage area, with velocities varying from <2 mm/yr to >8 mm/yr for a reference drainage area of 20 km^2 (given either faster propagation on steeper slopes or a particular erosional threshold). Given that the Paganica Catchment has

a drainage area five times larger than the reference area, the migration rate should be higher (e.g. Whittaker et al., 2008). Using a high migration rate of 1 cm/yr, the knickzone would be able to migrate 7.5 km upstream since the increase in fault slip rate. This is shorter than the actual distance between the knickpoint and the fault ($\sim$ 11.5 km), but is also a highly simplified estimate. Therefore, the possibility that the knickpoint is a transient response to increased slip on the Paganica Fault cannot be ruled out.

Knickpoint C, the last upstream of the Paganica Fault is located exactly on a lithological contact between limestone and alluvium on the ISPRA map (Fig. 2D), whereas Vezzani and Ghisetti (1998) mapped the fault upstream of this boundary. However, it is unlikely that a change in lithology alone could have caused the formation of the gorge observed upstream of this boundary, and most importantly, the lithological boundary is in all likeliness related to the fault itself. Therefore, it is more likely that the knickpoint is a response to an increase in slip rate on the Paganica Fault, rather than a change in lithology. If this is the case, then the migration rate has been significantly lower than what we estimated for the knickpoint at 7 km downstream. Nevertheless, this seems to be the most likely explanation for this knickpoint.

The Barete Catchment longprofile

The large convexity (D) in the Barete longprofile (Fig. 29) is located 16 km upstream of the Barete Fault (downstream distance = 5 km). Moving the knickpoint 16 km in less than 1 Myr, would take a very high migration rate. Using a high propagation rate of 1 cm/yr, the knickzone would still only be able to migrate 7.5 km upstream since the increase in fault slip rate about 0.75 Ma. It therefore seems less likely that the knickpoint in the Barete Catchment is caused by increased slip rates on the Barete Fault. A change in lithology from limestone to alluvium is observed between 8.5 to 9 km downstream, and another boundary to flysch lies quite close to the stream between 5.5 and 8.5 km downstream (Fig. 3D). As both alluvium and flysch is usually more easily eroded than solid limestone, a knickpoint may form as a response to such a change in lithology. However, as the distance between the knickpoint and the contact is >3 km, this also seems unlikely.

A final possibility is that the Montereale Fault is causing the knickpoint. The fault map by Roberts and Michetti (2004) shows a more elongated Montereale Fault, which the Barete Stream seems to be intersecting close to the knickpoint (Fig. 3). The map by Vezzani and Ghisetti (1998), however, has mapped a shorter Montereale Fault, which the Barete Stream may be intersecting at its southeastern tip. Naturally, errors in both maps regarding the position of the fault relative to the stream are possible, but even so, the damage zone of the Montereale Fault would be wide enough to include the Barete Stream. The Barete Fault in many aspects seems to be the most likely cause of the knickpoint (which will be discussed further in this chapter). Yet, very little data exists on this fault, so additional field work is necessary to explore this possibility.

Slope

Channel slope has been interpreted as one of the key variables that respond to tectonic signals (Whipple and Tucker, 2002). Empirical observations and simple models of fluvial erosion based on case studies of rivers in California and Nepal have suggested a positive correlation between slope and rock uplift rate (Wobus et al., 2006). Slope is therefore considered a key element in deciding whether or not rivers are affected by active tectonics. The Paganica Stream had steeper slopes upstream of the Paganica Fault (Fig. 16C). For the Barete Steam we cannot know how slope appears upstream of the Montereale Fault, but a very slight increase was observed upstream of the Barete Fault (Fig. 24C). This could indicate a transient response to the increasing uplift where both streams are steepening in attempt to make up for the change in slip. The increase in slope is evident within the Paganica Catchment, where incision has produced a very narrow and deep gorge. For the Barete Catchment the valley is slightly narrower upstream of the Barete Fault, but there are few signs of increased incision. Near the Montereale Fault, however, the steep and gorge-like reaches of the stream clearly indicate increased incision.

Bankfull channel width

The controls on channel width has for a long time been considered a major unresolved problem (Whipple, 2004), but some progress has been made on the subject. For a river in equilibrium, channel widt is expected to increase steadily as drainage area increases downstream. Channel width commonly increases with discharge and decreases with slope, and narrow channels are expected to respond faster to disturbances (Attal et al., 2008). A key observation for both studied streams was, that after initial widening in the headwater areas, channel widths remained mostly constant throughout both streams, even after large increases in drainage area (Figs. 16D and 24D). This corresponds with our observations of channel steepening before both faults. If higher uplift rates lead to steepening slopes, the channels will respond with narrowing to further increase their stream power (Whittaker et al., 2007b).

In Paganica, the channel was observed to be very narrow in the start of the gorge upstream of the Paganica Fault, possibly indicating a transient response. In Barete, however, channel widths became visibly wider just upstream of the Barete Fault, which seems like less of a transient response. Still, there were much fewer measurements along the Barete Stream, and this must be taken into consideration. Whittaker et al. (2007b) modelled channel widths using $W \sim A^{0.5}$, a model which assumes steady state. Using a constant of 0.015 for both catchments provided a nice fit in the headwater regions, but highly overestimated channel widths downstream (Fig. 29). The fact that a model assuming steady state ($W \sim A^{0.5}$) did not fit the data well, is another observation favouring that a transient response is occurring in both catchments.

Bankfull channel depth

Steepening slopes do not only lead to channel narrowing, but also deepening (e.g. Whittaker et al., 2007b). Increasing channel depths could therefore indicate a transient response to increasing fault slip. As the channel width is more or less constant throughout the Paganica Stream, we would expect the channel to be deepening further downstream as drainage area

increases. However, the channel depth plot also show constant values, and so we have a mass balance problem. This is likely related to water being extracted for farming further upstream. The Barete Stream has fewer channel depth measurements, but seems to be deepening right before the Barete Fault. An equilibrium stream would have a steadily deepening channel, different from what is observed for the Barete Stream, so the sudden deepening of the channel before the Barete Fault may indicate a transient response.

Unit stream power

Some detachment-limited models assume in their simplest form that fluvial incision is proportional to specific stream power (USP), which increases with narrower channels, steeper slopes and larger drainage area (Attal et al., 2011). The Paganica Catchment show a definite increase in USP (Fig. 16F), whereas the pattern for Barete (Fig. 24F) is more complex with two peaks in USP. By creating a USP map we are able to visualise the distribution of fluvial erosion rates (Fig. 30).

Both Barete and Paganica follow the same USP distribution pattern with a definite increase in USP, and thereby expected fluvial incision rate, just upstream of the faults. However, this pattern cannot be trusted completely as both streams are deprived of water because of human activity. For the Paganica Stream, the water flow was observed to decrease within and downstream of the farming areas. For Barete, continuously flowing water was first found downstream of the farming areas. Based on these observations, it seems that the USP values for Paganica should not be used as indicators of the current stream power distributions within the streas. They may represent how the stream power distribution would have been if the stream had been able to develop under "natural conditions", without disruptions of human activity.

Other than having lower values than Paganica, the USP plot for Barete (Fig. 24F) has a more abrupt peak before the Barete Fault, possibly indicating a transient response. The lack of measurements in the headwater reaches makes it difficult to predict the appearence of the USP in the area where the Barete Stream may be intersecting the Montereale Fault. Whittaker et al. (2007b) found that USP values would peak just upstream of the active fault for transient rivers, and then drastically decrease downstream. As we do not have any measurements downstream of the Paganica or Barete faults, we cannot compare the USP data to this statement. Also, it is important to bear in mind that as USP is highly dependent upon drainage area, thus the values will normally increase as long as area increases (assuming stable values of slope and channel width).

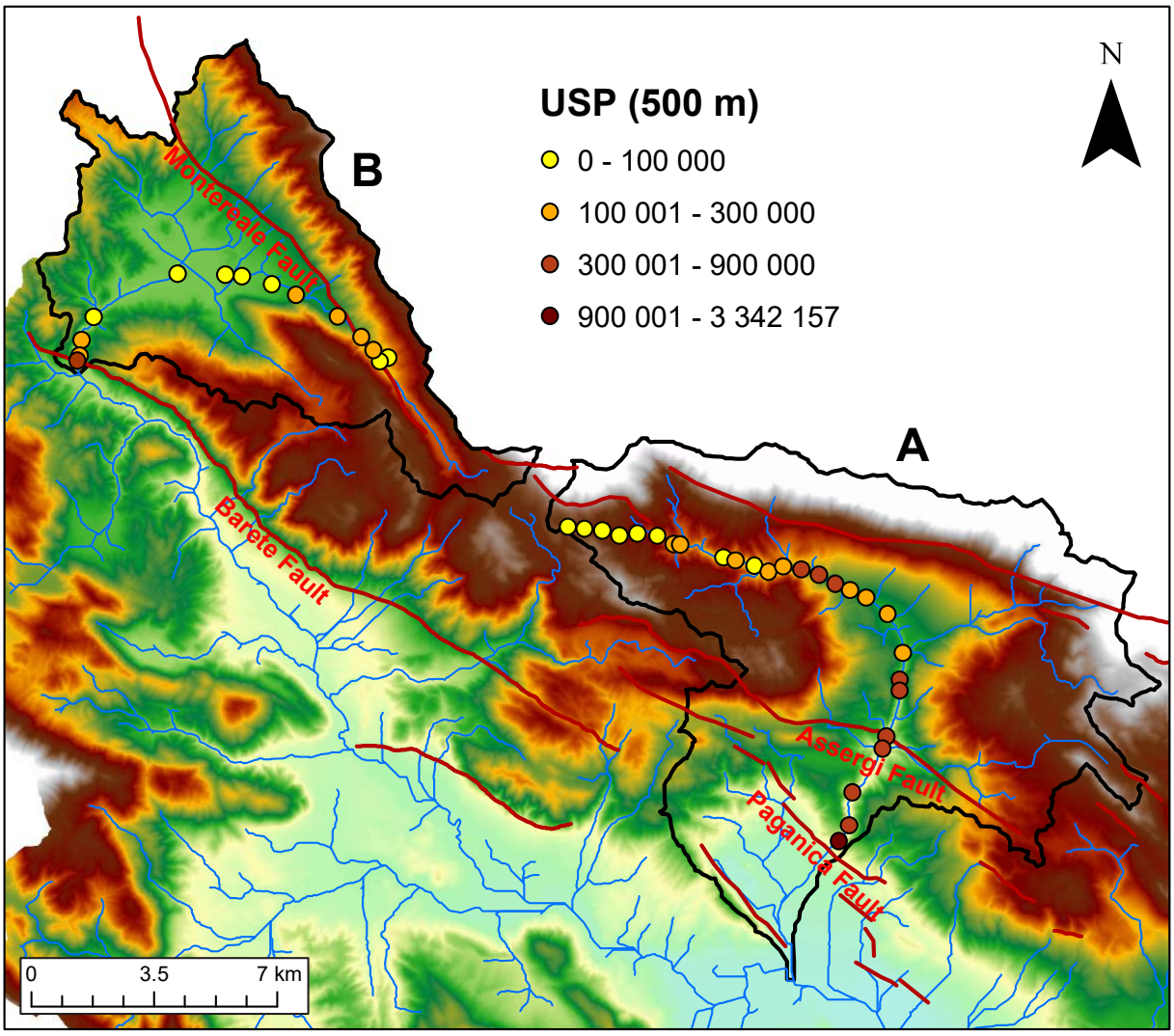

Fig. 30: The dots indicate USP values averaged over distances as close as possible to 500 m. The same pattern is observed for Paganica (A) and Barete (B): low values in the headwaters, followed by a slight increase. Values decrease as both streams turns toward the active faults, after which USP increases drastically towards the active fault.

Shear stress

For a transiently responding river, shear stress should increase close to the active fault. Attal et al. (2011) found that convexities propagate faster with higher shear stress. A simplified detachment-limited model assumes that fluvial incision is proportional to shear stress, which depends on river discharge, channel geometry, and that sediment is evacuated without influencing the river dynamics (Attal et al., 2011). Assuming this, the shear stress plots for Paganica (Fig. 16H) and Barete (Fig. 24H) indicate that both streams experience decreasing incision rates, except just upstream of the Barete and Paganica faults. A decreasing trend in shear stress is not common during a transient response and is in direct contrast to the USP plot, which shear stress commonly scales with.

As both streams appear to be deprived of water, the general decrease in shear stress is likely reflecting the present situation in the streams. The Paganica plot has a very high value at 17

km downstream, due to the steep slope and narrow channel width in the gorge. This might be an indication of how the shear stress would have been here, had the stream not been deprived of water further upstream. For Barete, shear stress peaks at the same distance as the knickpoint, which may again point to the nearby Montereale Fault. There is also a slight increase the last kilometres upstream of the Barete Fault. However, this is where continuously flowing water was observed in the channel for the first time, which may be the cause of this final increase.

Shields stress

Shields stress was a key element in the study by Whittaker et al. (2007b). They observed peaks in Shields stress based on D_{84} data upstream of an active fault, and a decrease further downstream. For Paganica, the Shields stress plot (Fig. 16I) also show peak D_{84} values in the intermediate reaches of the stream, but the values decline upstream of the Paganica Fault. Nevertheless, all values are well above the threshold value of 0.06 for transport-limited streams (Whittaker et al., 2007b, and references therein), thus most of the grain sizes are likely moving at bankfull flow. This may suggest that sediment size is not the dominant control on the channel slopes within the stream, similar to the observations of Whittaker et al. (2007b). Because Shields stress was only plotted for Paganica, the same conclusions may not hold for Barete.

Hack's law

The Hack's law plot for both Paganica (Fig. 17A) and Barete (Fig. 25A) features values fit for a river in topographic steady state. The Hack's constants for both streams are remarkably close to the "ideal" 0.6 value for equilibrium streams. Furthermore, all data points are more or less perfectly aligned ($R^2 > 0.9$). This is in sharp contrast to many other variables that indicate a transient response for both streams, and will be discussed further towards the end of this chapter.

Width-area correlation

For both catchments, the correlation between drainage area and channel width is weak (Figs. 17B and 25B). The width scaling exponent is much lower than 0.5, and therefore indicates a more transient response in both streams. However, both plots are poorly constrained with low R^2 values, thus, treated carefully, a constant width appoximately describes these channels.

Concavity

The concavity plots are very different for Paganica (Fig. 17C) and Barete (Fig. 25C), where the Paganica Stream has low concavity ($\theta \sim -0.2$) with low confidence ($R^2 = 0.33$), and the Barete Stream has a much higher concavity ($\theta \sim -1.0$) with high confidence ($R^2 = 0.73$). An equilibrium river is expected to have a concavity index close to 0.5. Kirby and Whipple (2001) relate concavities <0.4 with downstream increases in either rock strength or incision rates, and concavities between 0.7–1.0 with downstream decreases in rock strength or uplift rates. This would suggest that the Paganica Stream is experiencing increased incision downstream, which points to the Paganica Fault. For Barete, this suggests decreasing slip rates downstream, possibly

indicating that the Montereale Fault has a higher influence on the stream than the Barete Fault. However, as the studies by Kirby and Whipple (2001) are from compressional settings, this may not be directly transmitted to the extensional setting in the central Apennines. In any case, both streams display concavities in favour of a transient response. As described in Chapter 4.2.1, the Barete Catchment has particularly low slopes within the intermediate reaches. A possible explanation is that the Montereale Fault is back-tilting and rotating the footwall of the Barete Fault, flattening out the intermediate reaches of the Barete Catchment (Fig. 31). This would result in a higher concavity and lower slopes within the intermediate reaches of the stream.

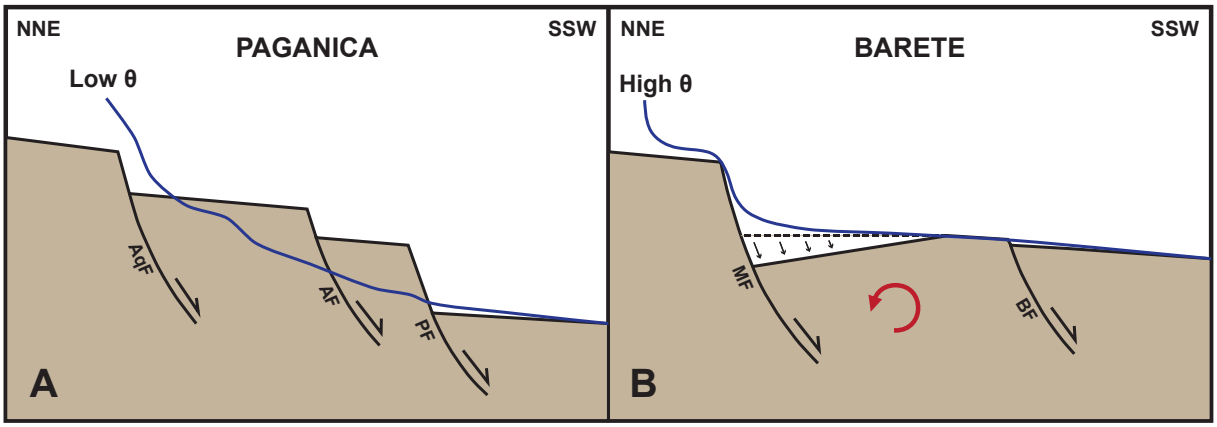

Fig. 31: Concept figure of the relative normal fault activity in the two catchments, and the possible effect on concavity. The river profiles are exaggerated for illustrational purposes. **A:** The concavity index (θ) for the Paganica Catchment is low. The structures are distributed as a more or less even staircase of normal faults (AqF = L'Aquila Fault, AF = Assergi Fault, PF = Paganica Fault). **B:** The very high concavity index (θ) for the Barete Catchment may be caused by back-tilting of the Montereale Fault (MF) hanging wall, which is also the Barete Fault (BF) footwall. This could explain the low slopes within the intermediate reaches of the Barete Stream.

Aspect ratio versus slope

Channel geometry largely controls landscape response time: channel width depends on slope, which again is controlled by uplift, and all are related to the migration rate of longprofile convexities (Attal et al., 2011). Aspect ratio is a highly non-linear function of slope for the Paganica Stream (Fig. 18), whereas the Barete Stream seems to have a more constant aspect ratio downstream (Fig. 26). Whittaker et al. (2007b) stated that for tectonically perturbed areas we cannot assume a constant aspect ratio, which means that the Paganica Stream show signs of a transient response, whereas the Barete Stream might be closer to topographic steady state. However, it is important to keep in mind the smaller number of data points for the Barete Stream, and the fact that both R^2 values are low (<0.3) for both streams.

Grain analyses

The transient response to fault uplift is associated with additional production and export of sediment, and more sediment equals more tools to erode the channel (Whittaker et al., 2010). Cowie et al. (2008) found that sediment supply has an effect equivalent to a 3–5 times increase

in shear stress. The Paganica Catchment was observed to contain much more sediment than the Barete Catchment, but the Barete Stream may have transported larger amounts of sediment in the past. However, examining the lithological map by Vezzani and Ghisetti (1998), large alluvial fan deposits are observed downstream of the Paganica Fault, but not in the downstream reaches of the Barete Stream. This suggests that the Barete Catchment has been – and still is – transporting less sediment. Also, the fact that a large portion of the sediment in Barete is flysch, indicates that the stream contains a large portion of sediment that is not as competent in eroding the channel. The Paganica Stream contained only limestone grains, which provides better tools for channel erosion. In summary: the Paganica Catchment seems to contain larger amounts of more competent tools for channel erosion. As the stream has eroded a deep gorge, it seems likely that this has also been the case in the past.

The large amount of sediment could also be the reason for the lack of large knickpoints in the Paganica Catchment; the deposits may have smoothed out the knickpoint, which was also observed by Cowie et al. (2008). Neglecting the effect of the relationship between sediment supply and transport capacity can obscure any simple correlation between channel slope and tectonics, and result in an active fault being interpreted as inactive or its relative uplift rate being highly underestimated (Cowie et al., 2008). As roundness was observed to increase downstream in both catchments, it is safe to assume that sediment is being transported through both streams. Grains are quite a bit smaller than in the analyses of Whittaker et al. (2007b), which could be reflecting a longer transport distance, or be an underestimate because of the method used (see Chapter 3.3.1). The increase in D_{84} within the intermediate reaches for Paganica is similar to the pattern observed by Whittaker et al. (2007b) for transient streams. However, the peak is not observed just upstream of the fault, and is therefore likely not related to the increasing slip rate. It is also important to keep in mind that the plot is based on a low number of measurements, and so the variations should be treated with caution.

Valley cross sections

The key feature among the Paganica cross sections is the distinct, M-shape produced by the gorge just upstream of the Paganica Fault. The fact that the valley widens immediately downstream of the Paganica Fault strongly suggest a connection between the fault and the gorge, favouring a transient response. The Barete cross sections are generally less dramatic than for Paganica. Even though the valley does narrow closer to the Barete Fault, there is no distinct gorge directly upstream of it. There is also less of an abrupt change in valley shape at the Barete Fault, suggesting that the slip generates less of a transient response for the Barete Stream. The most exceptional cross-section is the second one, close to where the Barete Stream may be intersecting the Montereale Fault. This is near the location of the knickpoint, and where steep reaches and bedrok incisions were observed in the field. This indicates that the Montereale Fault may have a stronger effect on the Barete Stream than the Barete Fault.

5.3 Summary of stream characteristics

Table 1 gives a schematic summary of the different variables that can be investigated to decide whether or not a river is undergoing a transient response.

Table 1: Whether or not a river is undergoing a transient response can be recognized by several factors. These are listed and reviewed for both studied streams. Most factors are in favour of a transient response (**YES**) for both streams, but some indicate equilibrium (**NO**) and for some factors it is difficult to define a clear trend (**Complex**). Based on Whittaker et al. (2007b).

Indications of a transiently responding river	**Paganica**	**Barete**
Longprofile with convexities	**YES**	**YES**
Slope increases towards the active fault(s)	**YES**	**YES**
Channel width decouples from drainage area/discharge, and narrows with higher slope and towards the active fault	**YES**	**NO**
Channel depth increases with higher slope and towards the active fault	**NO**	**YES**
Unit stream power increases towards the active fault	**YES**	**Complex**
Shear stress increases towards the active fault	**YES**	**YES**
Shields stress increases towards the active fault	**YES**	No data
Hack's constant, h≈ 0.6	**NO**	**NO**
The width-area scaling exponent, $\alpha \approx 0.5$	**YES**	**YES**
The concavity index, $\theta \approx 0.5$	**YES**	**YES**
Aspect ratio is a strongly non-linear function of slope	**YES**	**NO**
Grain size is coupled with hillslope input with D_{84} increasing upstream of the fault	**NO**	No data
Channel morphology characterised by: incision directly into bedrock, landslides directly feed the channel, steep hillslopes, deep gorges	**YES**	**Complex**

5.4 The dynamic state for the Barete and Paganica catchments

What becomes clear when observing Table 1 is that both streams have trademarks typical for both transient and equilibrium rivers. However, most of the parameters are in favour of a transient state for both streams. As most of central Italy may be described as undergoing a transient response due to the recent increase in tectonic activity ($\sim$ 0.75 Ma, Cowie and Roberts, 2001; Roberts and Michetti, 2004), it is not surprizing to find that these catchments show the same characteristics. What is curious is that both catchments also show qualities that

are characteristic for rivers in topographic steady state. What is the cause of these equilibrium characteristics?

Timing is an important aspect for analyses like these. It is possible that both streams have had enough time to adjust to the new boundary conditions, and are beginning to reach topographic steady state. As previously mentioned, it takes between 1 to 3 Myr for a catchment to adjust to new boundary conditions (Whittaker et al., 2007b), and fault acceleration occurred about 0.75 Ma (Roberts and Michetti, 2004). This would indicate a response time that is on the shorter end of the scale, but it is still plausible that some of the stream attributes would begin to approach equilibrium after 0.75 Myr. For the case of Hack's law, however, this is not necessarily the case.

5.5 Use of Hack's law in determining landscape transience

The plotting of Hack's law is the most puzzling dataset for each of the catchments, given the active tectonic setting. The nearly perfectly aligned data points and equilibrium values of Hack's constant do not match what the rest of the data seem to be indicating. Hack's law is among the most well-known scaling laws of river networks, and expresses the variation of average main stream length with drainage area (Dodds, 2000). For equilibrium rivers where erosion matches uplift, the power-law exponent, h, should be close to 0.6. Yet, is an exponent of 0.6 actually that difficult for a catchment to achieve? Would increased slip along a fault plane alone be able to change the length-area-correlation and provide a significantly different power-law exponent? The data collected in this study suggests otherwise.

For the two streams considered in this study, Hack's constant was 0.53 for Barete and 0.59 for Paganica. Consequently, even though the Paganica Stream seems to show more transient characteristics than the Barete Stream, judging from Hack's law, the Paganica Stream is even closer to equilibrium than the Barete Stream. If we consider the Rio Torto and the Penaro rivers (introduced in Chapter 2.1.5), Hack's constant is much lower for the transient Rio Torto, with h ~ 0.40, whereas for the steady state Penaro River h ~ 0.57 (Fig. 6A). Both plots have high R^2 values (~ 0.9), but the datapoints do not plot nearly as linearly as for the Paganica (Fig. 17A) and Barete (Fig. 25A) streams. The Penaro River may be considered a prime example of a stream in equilibrium. It is therefore interesting that the Barete and Paganica streams, showing definite signs of being in transient state, have similar, and even higher values of h compared to the Penaro River.

Dodds (2000) found that Hack's law has more complex features than usually implied by scientists, and that deviations of Hack's law are connected with basin size and shape, which is again determined by mountain building processes and faulting. Even subtle deviations from scaling were found to cause difficulties in determining exact scaling exponents. He concluded that the relation between basin area and stream length may be well described by scaling laws, but not for all cases, and that subtle correlations between basin shape and geologic features may produce deviations in Hack's law. Consequently, when it comes to Hack's law, relating theory, models and real stream networks is a great challenge (Dodds, 2000).

Based on these observations, the relevance of Hack's law in relation to determining landscape transience should perhaps be questioned. By plotting only Hack's law, the resulting Hack's exponent indicate topographic steady state for both the Barete and Paganica streams. Had this project not included field work, it would not be possible to observe locations of bedrock incision, landslides, steep slopes, narrow channel reaches and gorges in such detail, which are features that are key trademarks for transient rivers. By trusting Hack's law alone, both streams would have been concidered as being in topographic steady state, while this study shows that they are not. Hack's law does provide an excellent method for modelling relations between basins and stream networks, but may – in my opinion – not be the best indicator for the dynamic state of natural rivers.

There is, however, one possible explanation for the seemingly "perfect" values of Hack's constant. They could be a reflection of paleotopography. If the streams were present prior to the initiation of the normal faults (3 Ma, Cowie and Roberts, 2001; Roberts and Michetti, 2004), then these out of place values could be remnants from catchments that were previously in topographic steady state. After fault initiation, several stream properties would be able to respond quite fast (e.g. slope, channel dimensions, concavity, etc.), and after the increase in slip rates on the faults around 0.75 Ma, the transient signal should be further intensified. However, to significantly alter the length of the stream and the size of the drainage area would require a longer time period. This might explain why Hack's law is the only factor that irrevocably indicates topographic steady state. The subject of paleotopography is very interesting, and a further discussion on this will continue in the next section.

5.6 Are the two catchments interacting?

The headwaters of rivers that are best described as detachment-limited are vulnerable to loss of the upper part of the catchment during a transient response (if they are back-tilted) unless there is a rapid propagation of the incisional wave (Cowie et al., 2006; Whittaker et al., 2007b). The headwaters of the Barete and Paganica catchments are less than 1 km apart, and there is a possibility that one of the streams may be attempting to capture the other. Cowie et al. (2006) modelled the effects of fault growth on catchment development, and found that rivers crossing active faults tend to increase their headward erosion, which may often lead to capturing of other catchments. As rivers incise into the growing footwall, river capture events are suppressed even in the upper reaches, which eventually stabilises the catchment boundaries (Cowie et al., 2006).

Yet, why is there even a gap between the Barete and Paganica catchments? It seems strange that the two catchments do not already share a common drainage divide. Looking at the headwaters of Barete and Paganica (Fig. 32), another stream (X) is observed to have its headwaters between the Barete and Paganica catchments. This stream is shorter than the Barete and Paganica streams and seems to intersect the Barete Fault closer to its centre. Stream X is therefore likely affected by higher slip rates than the Barete Stream, which intersects the tip of the Barete Fault. It is possible that the stream has already captured parts of the headwaters of the Barete and Paganica catchments, as this could explain the gap between their headwaters.

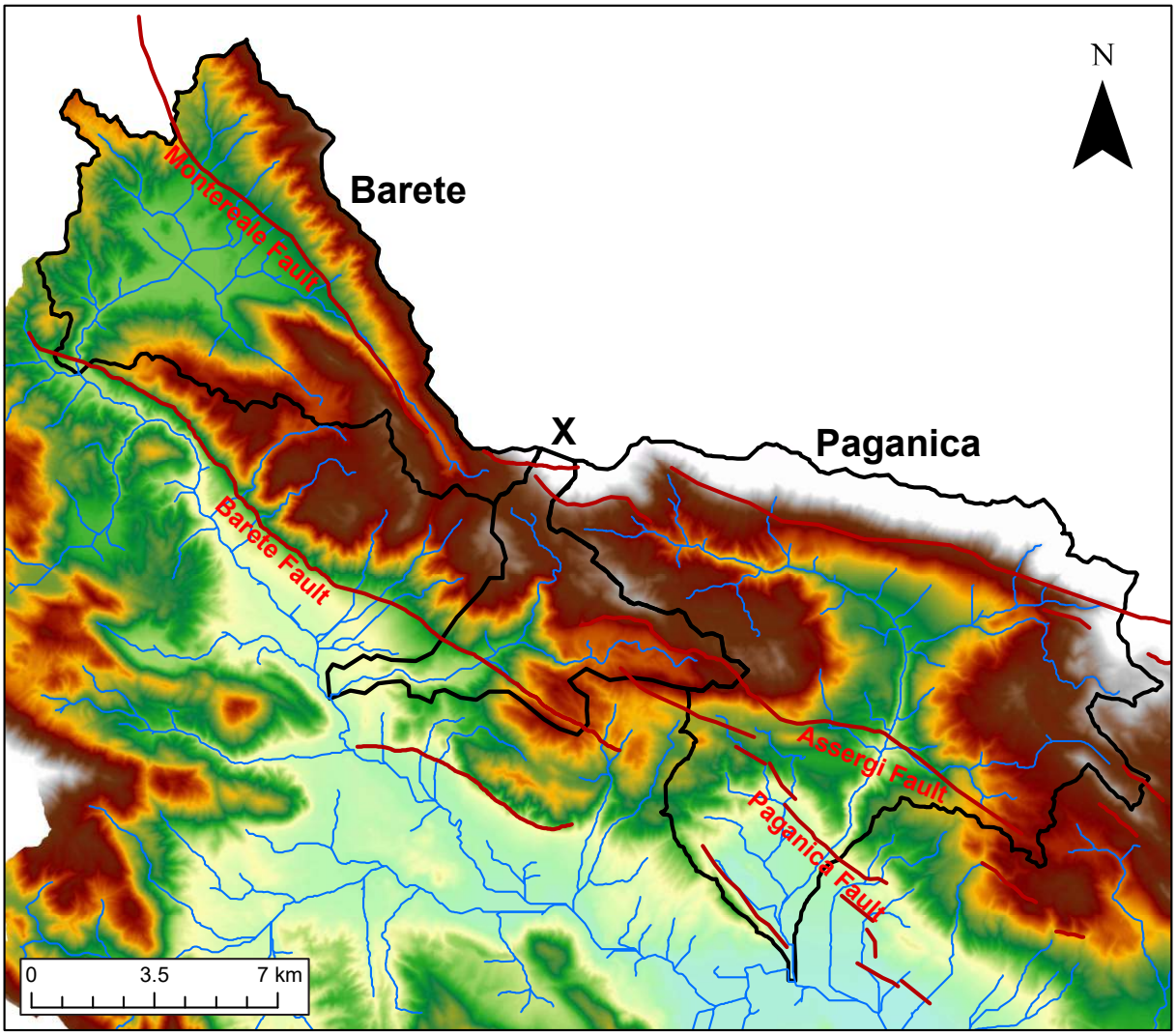

Fig. 32: Map showing the catchment (X) in between the headwaters of Barete and Paganica. As this third stream intersects the Barete Fault closer to its centre, it may be headward eroding both the Barete and Paganica catchments, atempting to capture their headwaters.

Headward erosion and capturing events could also possibly explain the current shape of the studied catchments. Looking at the other subcatchments within the Pescara Catchment (Fig. 8), it is evident that both the Barete and Paganica catchments have quite unique shapes. This might also be a consequence of aggressive heardward erosion by the smaller catchments along the Aterno River. Fig. 33 display two time steps: before and after fault initiation. Before fault initiation (<3 Ma) the Barete and Paganica catchments might have had more classic, rounded or pear-like shapes. After fault initiation, however, all catchments being affected by normal faults would increase their headward erosion, including the smaller catchments along the Aterno River. The smaller catchments would then be able to capture parts of the larger catchments, resulting in the more triangular-shaped catchments, similar to what is observed for Barete and Paganica.

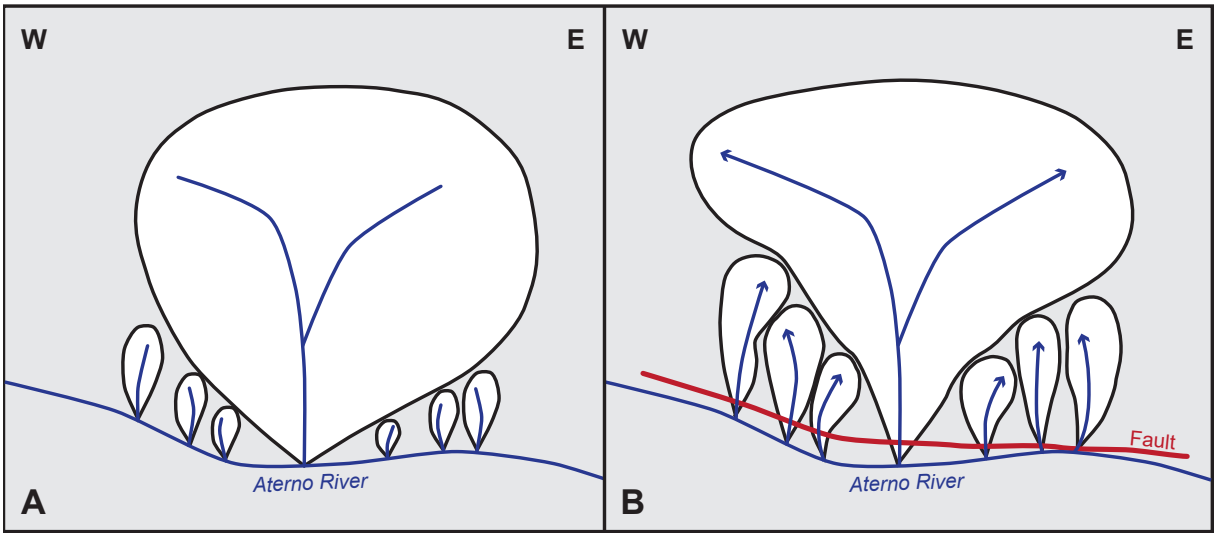

Fig. 33: Possible evolution of the Barete and Paganica catchments. **A:** Prior to fault initiation at 3 Ma, the Barete and Paganica catchments may have had classic, rounded shapes. **B:** After 3 Ma, fault initiation induces agressive headward erosion for all streams intersecting the normal faults. The smaller catchments would be able to headward erode into the larger catchments (Barete and Paganica), and capture parts of the stream network. Increased headward erosion would also cause elongation of the headwaters of the larger catchments, possibly resulting in more capturing events. This could be the explanation for the triangular-shaped Barete and Paganica catchments.

These speculations could be studied further by conducting a χ (Chi) analysis, a statistical technique for analysing longitudinal channel profiles (Mudd et al., 2014). Use of this method would make it possible to calculate the relative erosion rates of the different streams, which would help us to determine which of the catchments are more aggressive, and therefore most likely to be capturing the others. The method is also used to determine whether or not a stream is in equilibrium. Conducting a χ-analysis would therefore be interesting for a future research project, making it possible to verify the transient response of the Paganica and Barete streams, and to determine if they are being captured by surrounding catchments. Field investigations of the other catchments would also be useful. If this theory is correct, it may still be possible to observe the windgaps of the captured streams.

5.7 Predicting earthquake activity based on studies of fluvial geomorphology

Our analyses of the Paganica Catchment depicts a stream that is very likely to be highly affected by the active Paganica Fault. However, some factors point in the direction of equilibrium, and the knickpoints – as previously mentioned – are not that large. The slip rate estimated before the 2009 earthquake (0.6 mm/yr, Pace et al., 2006) is not exceptional relative to other faults in the region, and the fault was until 2009 a seldom mapped or recognized feature. However, the fact that other earthquakes of $M_w > 5$ have occurred on this fault in recent times (1461, 1762 and 1958, Pace et al., 2006) suggests that the fault is still highly active and could rupture again, resulting in earthquakes of similar magnitude.

By looking at the Paganica Stream alone, there are few geomorphological evidences of dramatic fault activity. There is no fault scarp at the locality where the stream intersects the fault, and the gorge upstream of the fault – though being an impressive feature – is not uncommon in the region. Also, the longprofile convexities are not as sharp as one would expect for a river intersecting a highly active fault. As previously discussed, this could be caused by the large amounts of sediment (tools for erosion), but the fact still stands: our data show very few "dramatic" features that could imply a fault that is very active. Naturally, this is a well known challenge for seismologists; predicting earthquake hazard is exceedingly difficult, especially regarding earthquake timing. Based on our observations that the stream shows signs of undergoing a transient response to increased slip on the Paganica Fault, and the fact that we know that large earthquakes have ruptured on this fault previously, we would expect more earthquakes to occur. Further predictions based on the fluvial geomorphology alone, however, would be speculative.

5.8 Sources of error

Human activity can be a major source of error when studying rivers running through urban areas. There are dams in both the Barete and Paganica catchments, which are obstacles for both water and sediment transport. However, they are most likely of modern times, and have therefore not been a major disturbance of the stream over time scales longer than a few hundred years. The major disruptions are the farmlands in both catchments where water is being removed, as well as road building and the channelized reaches of the streams. These factors make it challenging to interpret what the natural channel would look like, and may lead to poor measurements of channel geometry. They also affect water supply, stream power and thereby sediment transport, which somewhat obscures the natural appearence and behaviour of the stream. This is a clear disadvantage, but as most of the anthropogenic factors are of modern times, the only major inflictions are on the dimensions of the active channel.

The structural and lithological source material could contain errors that may lead to incorrect conclusions. Both geological maps may have errors and misplaced lithological boundaries. The older map by Vezzani and Ghisetti (1998) (Appendix 6) is not only a lithological map, but also show sediment depositions and fault traces, whereas the ISPRA map (Fig. 2D and Fig. 3D) strictly shows the bedrock lithology only. The overlay of the ISPRA map with the fault map of Roberts and Michetti (2004) may therefore not be perfectly accurate. The fault map by Roberts and Michetti (2004) was created by investigating the locations of faults on older geological maps. They state that misplacements of the fault traces are probable, with estimated error margins between 100-200 m perpendicular to the fault strike. As the locations of fault traces and lithological boundaries relative to the streams are essential in this study, errors like these must be taken into account.

Gaps in the downstream dataset are found for both rivers. The Barete Stream was difficult to access upstream of the knickpoint, and so there is a large gap in the data collection along the upstream reaches of the stream. Therefore we cannot know how the different datasets would plot

just upstream of the knickpoint and the possible intersection with the Montereale Fault. Having data from this area would help in determining the possible impact the Montereale Fault has on the stream. Still, the fact that most of the plots of S, W_b, USP and τ_b decrease downstream of the Montereale Fault, at least provides an indication that it may have some impact on the Barete Stream. Data is also missing downstream of the Paganica and Barete faults, because of the impact of human activity in the villages of Paganica and Marana. Observing how the data changes downstream of an active fault is an important factor for deciding whether or not the stream is responding to the increase in fault slip. However, the data for the Paganica and Barete streams within these villages would be highly inaccurate and were therefore not collected.

5.9 Implications for the regional landscape

Despite the small percentage river channels occupy relative to the total land surface, rivers dictate much of the topography of mountainous landscapes by setting the boundary condition for hillslope erosion (Whipple, 2004). The streams studied in this project have evolved over a long period of time prior to human interaction, and have eroded deep valleys and dramatic gorges. This clearly indicates that the streams must have carried more water in the past, and that the channels were somewhat deeper and wider. However, since the establishment of farmlands and villages along the streams, water has been extracted from the intermediate reaches, causing the channel dimensions of the 'modern' rivers to decrease. This also affects other stream properties (e.g. USP, shear stress, Shields stress), diminishing the transient response of the streams. However, this does not affect the dramatic topography of the landscape, which, together with detailed analyses of the stream properties and the DEM, strongly indicates that both catchments are undergoing a transient response to changing boundary conditions (i.e. increased fault slip rates).

This thesis provide several examples of what processes are at work in the central Italian Apennines at present: increasing slip rates on the normal fault array causes destabilizing of the catchments, which give rise to migrating channel convexities, headward erosion and the capture of nearby catchments. The catchments studied here are likely similar to how most of the catchments in central Italy appear: not completely transient, but a combination of several influences. Many features may in fact be remnants from before the development of the normal fault array.

This is a highly dynamic landscape, and further evolution of the Pescara Catchment is likely to involve more capturing events induced by headward erosion. Perhaps a total capturing of the Barete Catchment will cause the Aterno River to start further downstream? On the other hand, if the fault slip rates stabilize, the channel convexities will be able to migrate all the way upstream, leaving the system, so that the streams may regain their graded profiles, finally having reached topographic steady state.

6 Conclusions

This study presents detailed data on two streams in the tectonically active Abruzzo Region in central Italy. Through field work and digital analyses on a 10-m DEM, valley morphology, channel dimensions and a range of fluvial scaling relationships are reviewed.

The resulting data mostly indicate that both streams are undergoing a transient response to changing boundary conditions, caused by increased fault slip rates since ~ 0.75 Ma. Notable exceptions are shear stress and Shields stress, which are observed to generally decrease in both catchments, This is in direct contrast to the unit stream power plots, which shear- and Shields stress usually scale with. However, this is most likely a consequence of water being removed by irrigation in the farmland areas within the intermediate reaches of both streams, which is likely to have some effect on the characteristics of the present-day channel.

Another important exception is the plotting of Hack's law, the length–area-correlation, where the resulting plots indicate that both streams are in topographic steady state. This may indicate that Hack's law is inadequate for determining whether or not a stream is in topographic steady state. Another possibility is that the Hack's law plots are a reflection of paleotopography. If the streams were present before fault initiation, these values could be remnants from when the catchments were in topographic steady state. After fault initiation, several stream properties would be able to respond quite fast, whereas the length–area-correlation would take longer to adapt to the new boundary conditions.

Although the results are in favour of a transient response to increased slip rates, predicting earthquake events based on studies of fluvial geomorphology is a challenge. The topography of the catchments indicate the presence of active faults, and together with the knowledge that other large earthquakes have occurred on the faults, more high-magnitude ruptures would be expected to occur. However, any further predictions based on fluvial geomorphology alone, would be highly speculative.

The shape of the studied catchments may be caused by capturing events by the smaller nearby catchments, after fault initiation at 3 Ma. Capturing events caused by aggressive headward erosion by streams intersecting active normal faults seems to be one of the most important mechanisms of which the stream network is evolving in the central Italian Apennines. Further studies on possible capturing events would involve more field work, as well as χ analyses on relevant streams. This would increase our understanding of the inter-catchment dynamics within the Abruzzo Region, and possibly aid in predicting the future evolution of the entire Pescara Catchment.

References

Amato, A., Chiarabba, C., Selvaggi, G., 1997. Crustal and deep seismicity in Italy (30 years after). Annals of Geophysics 40 (5).

Anderson, H., Jackson, J., 1987. Active tectonics of the Adriatic region. Geophysical Journal International 91 (3), 937–983.

Attal, M., Cowie, P. A., Whittaker, A. C., Hobley, D., Tucker, G. E., Roberts, G. P., 2011. Testing fluvial erosion models using the transient response of bedrock rivers to tectonic forcing in the Apennines, Italy. Journal of Geophysical Research: Earth Surface (2003–2012) 116 (F2).

Attal, M., Tucker, G. E., Whittaker, A. C., Cowie, P. A., Roberts, G. P., 2008. Modeling fluvial incision and transient landscape evolution: influence of dynamic channel adjustment. Journal of Geophysical Research: Earth Surface 113 (F3).

Bagnaia, R., D'Epifanio, A., Sylos Labini, S., 1992. Aquila and Subequan basins: an example of Quaternary evolution in Central Apennines, Italy. Quaternaria Nova 2, 187–209.

Bigi, G and Cosentino, D and Parotto, M and Sartori, R and Scandone, P, 1992. Structural model of Italy and gravity map. Consiglio nazionale della ricerche.

Blumetti, A. M., Guerrieri, L., Vittori, E., 2013. The primary role of the Paganica-San Demetrio fault system in the seismic landscape of the Middle Aterno Valley basin (Central Apennines). Quaternary International 288, 183–194.

Castillo, M., Bishop, P., Jansen, J. D., 2013. Knickpoint retreat and transient bedrock channel morphology triggered by base-level fall in small bedrock river catchments: the case of the Isle of Jura, Scotland. Geomorphology 180-181, 1–9.

Cavinato, G. P., 1993. Recent tectonic evolution of the quaternary deposits of the Rieti Basin (Central Apennines, Italy): southern part. Geologica Romana 29, 411–434.

Cavinato, G. P., Cosentino, D., De Rita, D., Funiciello, R., Parotto, M., 1994. Tectonic-sedimentary evolution of intrapenninic basins and correlation with the volcano-tectonic activity in Central Italy. Memorie Descrittive Carta Geologica d'Italia 49, 63–76.

Cavinato, G. P., De Celles, P. G., 1999. Extensional basins in the tectonically bimodal central Apennines fold-thrust belt, Italy: response to corner flow above a subducting slab in retrograde motion. Geology 27 (10), 955–958.

Centamore, E., Nisio, S., 2003. Effects of uplift and tilting in the Central-Northern Apennines (Italy). Quaternary international 101-102, 93–101.

Charlton, R., 2007. Fundamentals of fluvial geomorphology. Routledge.

Cinti, F. R., Pantosti, D., De Martini, P. M., Pucci, S., Civico, R., Pierdominici, S., Cucci, L., Brunori, C. A., Pinzi, S., Patera, A., 2011. Evidence for surface faulting events along the Paganica fault prior to the 6 April 2009 L'Aquila earthquake (central Italy). Journal of Geophysical Research: Solid Earth 116 (B7).

Cowie, P. A., Attal, M., Tucker, G. E., Whittaker, A. C., Naylor, M., Ganas, A., Roberts, G. P., 2006. Investigating the surface process response to fault interaction and linkage using a numerical modelling approach. Basin Research 18 (3), 231–266.

Cowie, P. A., Roberts, G. P., 2001. Constraining slip rates and spacings for active normal faults. Journal of Structural Geology 23 (12), 1901–1915.

Cowie, P. A., Scholz, C. H., Roberts, G. P., Faure Walker, J. P., Steer, P., 2013. Viscous roots of active seismogenic faults revealed by geologic slip rate variations. Nature Geoscience 6 (12), 1036–1040.

Cowie, P. A., Whittaker, A. C., Attal, M., Roberts, G., Tucker, G. E., Ganas, A., 2008. New constraints on sediment-flux-dependent river incision: implications for extracting tectonic signals from river profiles. Geology 36 (7), 535–538.

D'Agostino, N., Jackson, J. A., Dramis, F., Funiciello, R., 2001. Interactions between mantle upwelling, drainage evolution and active normal faulting: an example from the central Apennines (Italy). Geophysical Journal International 147 (2), 475–497.

Dodds, P. S., 2000. Geometry of river networks. Ph.D. thesis, Massachusetts Institute of Technology.

Faccenna, C., Becker, T. W., Miller, M. S., Serpelloni, E., Willett, S. D., 2014. Isostasy, dynamic topography, and the elevation of the Apennines of Italy. Earth and Planetary Science Letters 407, 163–174.

Galli, P. A. C., Giaccio, B., Messina, P., 2010. The 2009 central Italy earthquake seen through 0.5 Myr-long tectonic history of the L'Aquila faults system. Quaternary Science Reviews 29 (27-28), 3768–3789.

Galli, P. A. C., Giaccio, B., Messina, P., Peronace, E., Zuppi, G. M., 2011. Palaeoseismology of the L'Aquila faults (central Italy, 2009, Mw 6.3 earthquake): implications for active fault linkage. Geophysical Journal International 187 (3), 1119–1134.

Gueguen, E., Doglioni, C., Fernandez, M., 1998. On the post-25 Ma geodynamic evolution of the western Mediterranean. Tectonophysics 298 (1-3), 259–269.

Hack, J. T., 1957. Studies of longitudinal stream profiles in Virginia and Maryland. U.S. Geol. Surv. Prof. Pap. 294B, 45–92.

Kirby, E., Whipple, K. X., 2001. Quantifying differential rock-uplift rates via stream profile analysis. Geology 29 (5), 415–418.

Lavecchia, G., Brozzetti, F., Barchi, M., Menichetti, M., Keller, J. V. A., 1994. Seismotectonic zoning in east-central Italy deduced from an analysis of the Neogene to present deformations and related stress fields. Geological Society of America Bulletin 106 (9), 1107–1120.

Malinverno, A., Ryan, W. B. F., 1986. Extension in the Tyrrhenian Sea and shortening in the Apennines as result of arc migration driven by sinking of the lithosphere. Tectonics 5 (2), 227–245.

Mudd, S. M., Attal, M., Milodowski, D. T., Grieve, S. W. D., Valters, D. A., 2014. A statistical framework to quantify spatial variation in channel gradients using the integral method of channel profile analysis. Journal of Geophysical Research: Earth Surface 119 (2), 138–152.

Pace, B., Peruzza, L., Lavecchia, G., Boncio, P., 2006. Layered seismogenic source model and probabilistic seismic-hazard analyses in central Italy. Bulletin of the Seismological Society of America 96 (1), 107–132.

Papanikolaou, I. D., Roberts, G. P., Michetti, A. M., 2005. Fault scarps and deformation rates in Lazio–Abruzzo, Central Italy: Comparison between geological fault slip-rate and GPS data. Tectonophysics 408 (1-4), 147–176.

Patacca, E., Sartori, R., Scandone, P., 1990. Tyrrhenian basin and Apenninic arcs: kinematic relations since late Tortonian times. Mem. Soc. Geol. It 45 (1), 425–451.

Pettijohn, F. J., Potter, P. E., Siever, R., 1973. Sand and Sandstone. Springer-Verlag, New York.

Powers, M. C., 1953. A new roundness scale for sedimentary particles. Journal of Sedimentary Research 23 (2).

Roberts, G., Raithatha, B., Sileo, G., Pizzi, A., Pizzi, S., Faure Walker, J. P., Wilkinson, M., McCaffrey, K., Phillips, R., Michetti, A., Guerrieri, L., Blumetti, A. M., Vittori, E., Sammonds, P., Cowie, P. A., 2010. Shallow sub-surface structure of the 6th April 2009 Mw 6.3 L'Aquila earthquake fault zone at Paganica, investigated with Ground Penetrating Radar. In: EGU General Assembly Conference Abstracts. Vol. 12. p. 5233.

Roberts, G. P., Michetti, A. M., 2004. Spatial and temporal variations in growth rates along active normal fault systems: an example from The Lazio–Abruzzo Apennines, central Italy. Journal of Structural Geology 26 (2), 339–376.

Selby, M. J., 1982. Rock mass strength and the form of some inselbergs in the central Namib Desert. Earth Surface Processes and Landforms 7 (5), 489–497.

Sklar, L., Dietrich, W. E., 1998. River longitudinal profiles and bedrock incision models: Stream power and the influence of sediment supply. Rivers Over Rock: Fluvial Processes in Bedrock Channels 107, 237–260.

Stampfli, G. M., 2000. Tethyan oceans. Geological society, london, special publications 173 (1), 1–23.

Szabó, T., Domokos, G., Grotzinger, J. P., Jerolmack, D. J., 2015. Reconstructing the transport history of pebbles on Mars. Nature Communications 6.

Tarboton, D. G., Bras, R. L., Rodriguez-Iturbe, I., 1991. On the extraction of channel networks from digital elevation data. Hydrological processes 5 (1), 81–100.

Tarquini, S., Vinci, S., Favalli, M., Doumaz, F., Fornaciai, A., Nannipieri, L., 2012. Release of a 10-m-resolution DEM for the Italian territory: Comparison with global-coverage DEMs and anaglyph-mode exploration via the web. Computers & Geosciences 38 (1), 168–170.

Valensise, G., Pantosti, D., 2001. Seismogenic faulting, moment release patterns and seismic hazard along the central and southern Apennines and the Calabrian Arc. In: Anatomy of an Orogen: The Apennines and Adjacent Mediterranean Basins. Springer, pp. 495–512.

Vezzani, L., Ghisetti, F., 1998. Carta Geologica Dell'Abruzzo [map], scale 1:100000. S.E.L.C.A., Firenze.

Whipple, K. X., 2001. Fluvial landscape response time: how plausible is steady-state denudation? American Journal of Science 301 (4-5), 313–325.

Whipple, K. X., 2004. Bedrock rivers and the geomorphology of active orogens. Annu. Rev. Earth Planet. Sci. 32, 151–185.

Whipple, K. X., Tucker, G. E., 2002. Implications of sediment-flux-dependent river incision models for landscape evolution. Journal of Geophysical Research: Solid Earth 107 (B2).

Whittaker, A. C., Attal, M., Allen, P. A., 2010. Characterising the origin, nature and fate of sediment exported from catchments perturbed by active tectonics. Basin Research 22 (6), 809–828.

Whittaker, A. C., Attal, M., Cowie, P. A., Tucker, G. E., Roberts, G., 2008. Decoding temporal and spatial patterns of fault uplift using transient river long profiles. Geomorphology 100 (3-4), 506–526.

Whittaker, A. C., Cowie, P. A., Attal, M., Tucker, G. E., Roberts, G. P., 2007a. Bedrock channel adjustment to tectonic forcing: Implications for predicting river incision rates. Geology 35 (2), 103–106.

Whittaker, A. C., Cowie, P. A., Attal, M., Tucker, G. E., Roberts, G. P., 2007b. Contrasting transient and steady-state rivers crossing active normal faults: new field observations from the Central Apennines, Italy. Basin Research 19 (4), 529–556.

Wobus, C., Whipple, K. X., Kirby, E., Snyder, N., Johnson, J., Spyropolou, K., Crosby, B., Sheehan, D., 2006. Tectonics from topography: Procedures, promise, and pitfalls. Geological Society of America Special Papers 398, 55–74.

Zaprowski, B. J., Pazzaglia, F. J., Evenson, E. B., 2005. Climatic influences on profile concavity and river incision. Journal of Geophysical Research: Earth Surface 110 (F3).

Appendices

Appendix 1 - Paganica dataset

Appendix 2 - Barete dataset

Appendix 3 - Table explanations for appendices 1 and 2

Appendix 4 - Rock mass strength form

Appendix 5 - Grain descriptions

Appendix 6 - Geological map of the Abruzzo Region

Appendix 1 - Paganica dataset

Loc.	X	Y	Elevation				Dist:	Length		A	Slope		H_b	W_b	R_h	Setting	RMS	Grain size	
			GPS	DEM_l	DEM_p	var.	l-p	dfd	dfh		field	fit						D_{50}	D_{84}
0				1467.0	1467.0			0.0	-653.0	0						divide			
2-1	0367020	4701065	1473	1463.5	1460.3	12.7	8.5	49.0	-49.0	9104		0.04				plain			
2-2	0367553	4700782	1441	1437.3	1434.4	6.6	2.8	653.3	0.0	578317		0.07	0.10		0.06	transition			
2-3	0367600	4700760	1438	1437.3	1432.5	5.5	1.2	705.3	52.0	599685		0.09	0.50		0.21	transition			
2-4.1	0367883	4700701	1412	1417.7	1415.6	5.7	0.4	994.7	341.5	761805		0.06				valley			
2-4.2	0367922	4700705	1409	1412.3	1412.9	3.9	7.5	1034.0	380.7	766851		0.14				valley			
2-5	0367976	4700696	1407	1407.6	1407.6	0.6	0.3	1088.8	435.5	862655		0.07				valley			
2-6.1	0368005	4700703	1403	1409.0	1405.6	6.0	5.7	1118.7	465.4	1633813	0.22	0.25				valley			
2-6.2	0368019	4700699	1400	1403.1	1403.1	3.1	2.7	1133.3	480.0	1636076		0.13				valley			
2-7	0368133	4700684	1382	1395.8	1389.0	13.8	15.8	1248.4	595.1	1666261		0.11				valley			
2-8	0368176	4700684	1377	1393.2	1382.1	16.2	18.9	1291.5	638.2	1696589		0.17				valley			
2-9	0368212	4700673	1372	1380.6	1377.6	8.6	10.4	1329.2	675.9	1707143		0.16				valley			
2-10	0368225	4700673	1369	1374.2	1375.7	6.7	11.3	1342.2	688.9	1707315		0.83				transition			
2-11	0368231	4700675	1366	1374.2	1374.0	8.2	13.8	1348.5	695.2	1707448		0.08		2.0±0.5		gorge			
D3a	0368509	4700607	1335	1341.7	1341.7	6.7	3.6	1632.9	979.7	1890318		0.09				gorge			
3-1	0368541	4700577	1324	1341.5	1336.5	17.5	32.2	1679.1	1025.8	1902276	0.10	0.08	0.75±0.25	1.5±0.5	0.38	valley			
D3b[1]	0368661	4700611	1316	1320.4	1321.9	5.9	15.3	1804.0	1150.7	2004344		0.09				valley			
D3c	0368678	4700609	1312	1317.9	1315.8	5.9	13.3	1821.1	1167.9	2004376		0.11				valley			
D3d	0368769	4700594	1304	1305.3	1303.1	2.2	10.9	1913.5	1260.2	2756406		0.10				valley			
D3e	0368785	4700581	1300	1299.9	1299.9	0.1	0.0	1934.1	1280.9	2777638		0.13				valley			
3-2	0368830	4700535	1293	1292.6	1292.6	0.4	0.5	1998.6	1345.3	2808612		0.13				valley			
3-3	0368856	4700521	1289	1289.0	1289.2	0.2	8.1	2028.1	1374.9	2903748	0.03	0.12	1.00±0.25	4.0±1.0	0.40	valley			
D3f	0368989	4700431	1277	1275.4	1273.5	3.5	18.1	2189.0	1535.7	3004877		0.08				valley			
3-4	0369270	4700401	1245	1246.8	1245.4	1.8	13.6	2472.0	1818.7	3829378		0.08				valley			
3-5	0369507	4700465	1224	1226.6	1226.8	2.8	23.9	2717.8	2064.5	3894666		0.08	0.50±0.25	2.0±0.5		valley		21.59	36.11

[1]D = dam

Loc.	X	Y	Elevation				Dist:	Length		A	Slope		H_b	W_b	R_h	Setting	RMS	Grain size	
			GPS	DEM_l	DEM_p	var.	l-p	dfd	dfh		field	fit						D_{50}	D_{84}
D3g	0369708	4700501	1209	1197.3	1197.4	11.7	5.5	2922.3	2269.0	4589296		0.11				tributary			
3-6	0369759	4700475	1204	1194.6	1191.2	12.8	19.1	2979.6	2326.3	6206111		0.08				valley			
3-7	0370071	4700346	1175	1168.4	1161.0	14.0	42.0	3317.7	2664.4	6640336		0.07				valley			
3-8	0370228	4700245	1163	1156.0	1148.4	14.6	62.6	3504.7	2851.4	6690300		0.08				tributary			
3-10	0370391	4700136	1144	1140.3	1138.7	5.3	16.0	3701.0	3047.8	6956309	0.05	0.06	1.25±0.25	7.00±1.00	0.92	spring		13.44	27.29
2-12	0370508	4700089	1143	1137.3	1132.5	10.5	22.1	3827.3	3174.0	6998749	0.06	0.11	1.00±0.50	6.00±1.00	0.75	valley			
3-11	0370691	4700057	1133	1124.2	1123.6	9.4	10.5	4013.3	3360.1	8019957	0.06	0.03	1.25±0.25	7.00±1.00	0.92	valley		23.05	34.67
4-8	0371889	4699607	1074	1071.4	1068.4	5.6	15.8	5294.9	4641.6	17558405	0.04	0.03	0.50±0.25	2.50±0.50		valley			
4-9	0372116	4699547	1068	1063.6	1058.9	9.1	16.6	5530.0	4876.8	17709631		0.09			0.83	scree			
4-7	0372226	4699497	1064	1059.3	1054.8	9.2	11.7	5651.0	4997.8	18350052	0.05	0.03	1.25±0.25	5.00±1.00	0.42	valley			
4-10	0372752	4699310	1043	1038.8	1034.7	8.3	16.9	6210.1	5556.8	18721193	0.01	0.02	0.50±0.25	5.00±1.00		valley			
4-6	0372900	4699206	1044	1027.9	1027.9	16.2	3.2	6391.3	5738.0	19400237		0.03				tributary			
4-5	0372997	4699153	1039	1032.4	1023.8	15.2	20.1	6502.0	5848.7	24233911		0.04	1.00±0.50	8.00±2.00		valley			
4-4	0373038	4699115	1038	1023.2	1023.2	14.8	9.3	6557.9	5904.7	25001647		0.08				tributary			
4-3	0373138	4699108	1031	1022.3	1019.4	11.6	9.7	6658.3	6005.0	25047862		0.09				valley			
4-11	0373243	4699086	1014	1019.9	1016.1	5.9	11.5	6765.8	6112.5	25096434		0.10				spring			
4-12	0373333	4699140	1009	1014.3	1012.5	5.3	7.2	6869.3	6216.0	25169229		0.06				valley			
4-1.4	0373570	4699230	997	1004.1	1004.1	7.1	2.9	7120.0	6466.0	25386781	0.08	0.04	0.75±0.25	5.50±0.50	0.59	valley			
4-1	0373570	4699230	997	1004.1	1004.1	7.1	2.9	7124.8	6471.5	25386781	0.08	0.04	0.75±0.25	5.50±0.50	0.59	valley			
4-1.1	0373570	4699230	997	1004.1	1004.1	7.1	2.9	7125.0	6471.0	25386781	0.08	0.04	0.75±0.25	5.50±0.50	0.59	valley			
4-1.2	0373570	4699230	997	1004.1	1004.1	7.1	2.9	7130.0	6476.0	25386781	0.08	0.04	0.75±0.25	6.00±0.50	0.60	valley			
4-1.3	0373570	4699230	997	1004.1	1004.1	7.1	2.9	7140.0	6486.0	25386781	0.08	0.04	0.75±0.25	6.00±0.50	0.60	valley			
4-14	0373885	4699163	983	975.6	975.6	7.4	2.0	7447.3	6794.0	30222927		0.05				valley			
4-15	0374076	4699099	972	971.1	966.4	5.6	17.3	7649.0	6995.7	30454657		0.07				valley	40		
4-16	0374259	4699029	961	962.9	957.6	5.4	18.3	7845.2	7191.9	30711322		0.05				valley			
9-1	0374560	4698924	935	943.6	936.5	8.6	28.7	8164.5	7511.2	32595229	0.02	0.06	0.75±0.25	6.00±0.50	0.60	valley		21.41	39.05

Loc.	X	Y	Elevation				Dist:	Length		A	Slope		H_b	W_b	R_h	Setting	RMS	Grain size	
			GPS	DEM_l	DEM_p	var.	l-p	dfd	dfh		field	fit						D_{50}	D_{84}
4-17	0374610	4698926	939	935.1	933.6	5.4	4.9	8214.6	7561.3	32608410		0.10				valley			
9-2	0374661	4698871	930	929.1	927.1	2.9	3.9	8289.7	7636.4	32647768		0.04				valley			
9-3	0374685	4698867	930	929.0	926.0	4.0	18.9	8314.1	7660.8	32648405	0.02	0.04	0.75±0.25	14±1.0	0.68	valley			
9-4	0374701	4698824	933	923.4	923.4	9.6	1.6	8360.0	7706.8	32666502		0.02		9.0±1.0	0.45	valley			
9-5	0374766	4698777	928	923.1	920.4	7.6	17.8	8440.4	7787.1	33352370		0.04	2.00±0.50	5.0±1.0	1.11	valley		32.26	62.12
9-6	0374830	4698714	924	921.0	916.5	7.5	18.2	8530.3	7877.0	33417609	0.05	0.05	1.25±0.25	5.0±1.0	0.83	transition			
9-7	0375014	4698642	917	921.3	907.8	13.5	40.5	8728.2	8074.9	35284257	0.12	0.03				transition			
9-8	0375419	4698427	900	897.9	892.3	7.7	25.0	9187.4	8534.1	38151483		0.03			0.50	plain			
9-9	0375854	4698179	885	872.4	872.4	12.6	7.7	9688.9	9035.6	40418998	0.03	0.03	0.75±0.25	3.0±1.0		plain		13.92	56.58
9-10	0376101	4698022	878	869.7	866.5	11.5	29.4	9982.0	9328.7	42847428		0.03				plain			
D9b	0376437	4697677	868	852.8	852.8	15.2	4.3	10464.3	9811.0	43797956		0.02				plain			
9-11	0376779	4696535	837	828.2	822.9	14.1	19.3	11658.2	11004.9	77522729	0.01	0.03	0.40±0.10	5.0±1.0	0.34	plain			
D9b	0376817	4696389	827	818.6	818.6	8.4	1.1	11809.3	11156.0	77616630		0.04				plain			
9-12	0376639	4695781	809	805.0	801.9	7.1	16.3	12443.7	11790.5	78672853		0.03	0.50±0.10	3.0±0.5	0.38	plain			
9-13	0376623	4695475	801	797.0	794.6	6.4	21.9	12750.6	12097.3	79047387		0.02	0.40±0.10	3.5±0.5	0.33	plain	61		
10-8	0376144	4694203	766	761.8	761.8	4.2	7.2	14111.9	13458.6	84963900	0.01	0.02	1.25±0.25	9.0±1.0	0.98	plain			
1-2	0376027	4693864	754	751.5	751.1	2.9	29.0	14471.0	13817.7	85093226	0.00	0.02	0.40±0.10	3.0±0.5	0.32	plain		15.92	24.71
10-4	0375086	4692689	729	720.5	720.5	8.5	4.0	15978.6	15325.3	110372239		0.02			0.45	transition			
D10a	0374917	4691749	710	702.2	701.7	8.3	7.1	16935.1	16281.8	111529511		0.03	0.60±0.25	3.5±0.5	0.56	transition		15.56	32.95
1-5.3	0374888	4691710	695	699.3	699.3	4.3	4.7	16983.8	16330.5	111691096		0.15	1.00±0.25	2.5±0.5		gorge			
1-5.2	0374838	4691662	694	695.7	695.7	1.7	1.7	17053.2	16399.9	111723322		0.04				gorge			
1-5.1	0374801	4691593	692	691.9	692.6	0.6	2.5	17131.6	16478.3	111738827		0.00				gorge			
9-14	0374752	4691510	695	685.4	685.4	9.6	3.0	17228.1	16574.8	111828502	0.02	0.02	1.00±0.50	6.0±1.0	0.75	gorge	77		
12-1.1	0374596	4691340	695	677.1	673.2	21.8	25.3	17459.2	16805.9	111957746		0.03	1.25±0.25	4.5±0.5	0.80	gorge			
12-1.2	0374265	4691076	669	663.9	663.9	5.1	1.2	17883.2	17229.9	112165388		0.00		9.0±1.0		P. Fault[2]			
Conf.[3]				584.0	584.0	0.0		23060.8	22407.8	138423545						confluence			

[2]P. Fault = Paganica Fault

[3]Conf. = confluence

Appendix 2 - Barete dataset

Loc.	X	Y	Elevation				Dist:	Length		A	Slope		H_b	W_b	R_h	Setting	RMS
			GPS	DEM_l	DEM_p	var.	l-p	dfd	dfh		field	fit					
0	365595	4701656			1434			0.0		0		0.26				divide	
13-18	364990	4702182	1290	1296	1293	6	5	743.1		305000		1.55				valley	
13-8	362784	4705950	1096	1095	1093	3	10	250.0		19400	0.21	0.05	0.40	4.00	0.33	tributary	
13-10	362548	4705851	1043	1023	1020	23	20	5265.7		9241100	0.09	0.01	0.65	4.00	0.49	valley	
13-11	362517	4705874	1035	1027	1018	17	25	5304.3		9250800		0.11				valley	
13-12	362481	4705932	1031	1017	1014	17	10	5372.6		9298700		-0.01				valley	
13-13	362430	4706007	1037	1016	1012	25	5	5463.3		9376400		0.07	1.00	6.00	0.75	valley	
13-14	362392	4706189	1009	996	995	14	50	5675.8		9522900		0.13				tributary	
13-15	362262	4706339	989	985	987	4	15	5843.7		10594200	0.04	0.08	0.80	5.00	0.61	valley	
13-16	362190	4706434	987	983	977	10	15	5962.9		10616000		0.07				valley	
13-7	362079	4706578	968	972	965	7	20	6165.2		10956500	0.01	0.05	0.75	1.50	0.38	valley	62
13-17	361440	4707213	928	916	916	12	5	7116.1		12928000		0.04				transition	
13-6	360309	4707909	872	871	866	6	70	8574.5		17030600		0.04				transition	58
13-5	359966	4708057	859	855	853	6	135	8950.7		17189200		0.03	0.85	4.50	0.62	plain	
13-4	359640	4708255	850	843	844	7	140	9332.1		17343800		0.02				plain	
13-3	358808	4708554	834	830	829	5	35	10218.8		22879100	0.00	0.02	0.50	3.25	0.38	plain	
13-2	358339	4708626	828	828	826	2	240	10693.5		24943700	0.00	0.01	0.65	3.50	0.47	plain	
13-1	356988	4708756	822	817	816	6	110	12050.9		66579800	0.00	0.00	0.50	5.00	0.42	plain	
13-20	354523	4707693	817	813	803	14	55	14771.6		76139300		0.00	2.25	9.00	1.50	valley	
13-21	354136	4707067	809	797	796	13	10	15584.2		78097400		0.01	3.00	9.00	1.80	valley	
13-22	354036	4706619	804	793	792	12	10	16137.4		78855400		0.01	3.00	9.00	1.80	valley	
B. Fault[4]	353982	4706485			791			16296.4		78992900		0.03				B. Fault	
Conf.	354003	4706103			787			16705.5		79370200		0.00				confluence	

[4]B. Fault = Barete Fault

Appendix 3 - Table explanations for appendices 1 and 2

Title	Explanation
Loc.	Locality recorded in notebook
X	X GPS-coordinate
Y	Y GPS-coordinate
Elevation GPS	Elevation measured in the field by GPS (masl)
Elevation DEM l	Elevation at field locality measured on the DEM (masl)
Elevation DEM p	Elevation at locality in the stream on the DEM (masl)
Elevation var.	Variability between different elevation measurements (m)
Dist: l-p	Distance between GPS locality and the stream on the DEM (m)
Length dfd	Distance from drainage divide (m)
Length dfh	Distance from channel head (m)
A	Drainage area (m^2)
Slope field	Slope measured in the field (dZ/dL) (m/m)
Slope fit	Slope calculated in MATLAB (m/m)
Hb	Bankful depth (m)
Wb	Bankful width (m)
Rh	Hydraulic radius (m)
RMS	Selby rock mass strength index
Grain size D_{50}	Median grain-size (mm)
Grain size D_{84}	Coarse-fraction grain-size (mm)

Appendix 4 - Rock mass strength form

	Rock mass strength classification								Elevation				x				y					
1	Rock strength (Schmidt Hammer)																					
	1	2	3	4	5	6	7	8	9	10	11	12	13	14	15	16	17	18	19	20		
r	if > 60, r = 20				if 50-60, r = 18				if 40-50, r = 14				if 35-40, r = 10				if 10-35, r = 5					
2	Weathering																					
	Unweatherd				Slightly				Moderately				Highly				Completely					
r	10				9				7				5				3					
3	Spacing of joints																					
	> 3 m				3 - 1 m				1 - 0.3 m				300 - 50 mm				< 50 mm					
r	30				28				21				15				8					
4	Joint orientation																					
	Steep dips into slope				Moderate dips into slope				Horizontal or nearly vertical dips (hard rocks only)				Moderate dips out of slope				Steep dips out of slope					
r	20				18				14				9				5					
5	Width of joints																					
	< 0.1 mm				0.1 - 1 mm				1 - 5 mm				5 - 20 mm				> 20 mm					
r	7				6				5				4				2					
6	Continuity of joints																					
	None				Few				Continuous, no infill				Continuous, thin infill				Continuous, thick infill					
r	7				6				5				4				1					
7	Outflow of ground water																					
	None				Trace				Slight				Moderate				Great					
r	6				5				4				3				1					
																						0
	Total rating																					
	Very strong		100-91																			
	Strong		90-71																			
	Moderate		70-51																			
	Weak		50-26																			
	Very weak		<26																			

Appendix 5 - Grain descriptions

Photo	Roundness*	Sphericity	Sorting	Description of locality
3-5.4	M = 2.9	Low	Moderate	End of small gorge. Dry, narrow and shallow channel. Steep valley sides exposing weathered limestone.
3-10.1	M = 3.5	Low to intermediate	Poor to moderate	Dry, narrow and shallow channel. Stone walls built on either side of the stream, and large boulders have fallen in.
3-11.b3	M = 3.0	Low	Moderate to well	Wide valley. Channel filled with water. Nice gravel bars. A lot of sediment is added by a dry side stream.
9-1.1	M = 3.5	Low	Moderate to well	Narrow valley. In a forest where the whole floor is covered with sediments. The active channel is wide and shallow.
9-5.3	M = 3.8	Intermediate	Poor	Downstream of an incised bend in the stream. Nearby valley side exposes weathered limestone overlain by cemented alluvium with rounded limestone clasts.
9-9.3	M = 4.0	Low to intermediate	Moderately	In the farmlands. The stream is narrow and shallow, and water is frequently being removed to water crops.
1-2.1	M = 4.4	Low	Moderate to poor	In the farmland areas near Assergi, underneath a bridge. The channel is narrow and shallow.
9.-11.1	M = 4.1	Low	Poor to moderate	In the big turn of the stream downstream of Assergi. Small sediment bars, a lot of sand and vegetation.
Dam 10A.2	M = 4.1	Low	Poor	Narrow valley. Downstream of a 1 m high dam. Large gravel bars. The gorge is 50 m further downstream.

* Mean value

Appendix 6 - Geological map of the Abruzzo Region

A section of the map *Carta Geologica Dell'Abruzzo*. The overlain catchment boundaries for Barete and Paganica are approximate. For legends and scale, see full map by Vezzani and Ghisetti (1998).